Near-source response of a resistive layer to a vertical or horizontal electric dipole excitation

Nestor H. Cuevas[1] and David Alumbaugh[2]

ABSTRACT

Frequency and time-domain analytical expressions are derived for the electromagnetic field response of a resistive layer inserted in an otherwise homogeneous whole-space as observed in the vicinity of an electric dipole source. The analysis of closed-form solutions demonstrated that at near-source-receiver offsets, the spectral and spatial distribution of the fields is better described by a superposition of images, associated with the dipolar character of the charges distributed in the boundaries, rather than the *guided mode* behavior dominating the response in the far offset regime. Approximate solutions of the fields in the frequency domain were derived using the saddle point method of integration. The formulas describing the fields were in good agreement with semianalytical calculations. However, a lower frequency bound was found, below which the expressions are inaccurate, and thereby they cannot be used to obtain time-domain solutions. A kernel modulation scheme was used instead, which yields an infinite series representation for the fields. The expressions thus derived produce accurate fields to very low frequencies, and thereby they were also used to obtain time-domain formulas. The analysis indicated that for a vertical electric dipole (VED) excitation, the late time response of the *image field* associated with the charge density induced on the upper boundary appears to cancel the direct field, thus providing the response of the layer. For a horizontal electric dipole (HED) source, the superimposed contributions of the transverse electric (TE) and transverse magnetic (TM) modes appeared to oppose the *image field*, resulting in the direct field dominating over the response of the layer, and thereby masking any sensitivity to the properties of the layer in this configuration.

INTRODUCTION

In marine controlled-source electromagnetic (CSEM) hydrocarbon exploration, an electromagnetic (EM) source is used to excite the subsurface by radiating low-frequency energy and simultaneously recording the resulting EM fields as a function of time and/or space. What has become known as the standard CSEM method or sea bed logging (SBL) consists of a towed (e.g., more than 200 m long) antenna emitting harmonic (e.g., frequency 0.25 Hz) energy, and an array of stationary receivers, spaced at 1–3 km over a 10–30-km line, recording two to five components of the electromagnetic fields in the sea bottom (Eidesmo et al., 2002). In practice, an SBL data set consists of the electromagnetic fields measured in the seafloor, at discrete frequencies (Mittet and Schaug-Pettersen, 2008), as the source traverses the survey area. This results in a geometrical sounding of the fields that yields a stronger target response and greater depth of investigation with increasing source-receiver offset.

Recently, a vertical source-receiver time-domain measurement has emerged as an alternative method (Barsukov et al., 2007). In this case, a long period (more than 200 s, 50% duty cycle) waveform is continuously transmitted by a stationary vertical antenna (length dependent on water depth) while the vertical component of the electric field is recorded at a fixed, nearby seafloor receiver. The data set is obtained by postprocessing of the time series to recover a stacked waveform, and hence, extract the field's transient decay. The response from deep reservoirs appears at increasingly late times, even at very close source-receiver offsets (see Figure 1b, 1a for a numerical example), and therefore, the method can be used (given a favorable signal to noise ratios) to discriminate deep resistive targets.

In the SBL method, the spatial dependence of the field at offsets of 2–10 km is the dominant reservoir detection mechanism, thus the source can be towed leading to certain acquisition efficiency. With the transient measurement, the fields need to be recorded

and stacked out to 30 to 100 s after the shutoff of the current, at relatively close offsets. This requires a stationary source position and extended measurement intervals to achieve required signal to noise, which in turn, leads to acquisition inefficiency. Naturally, the question arises regarding the performance of each technique and thereby the fundamental understanding of the behavior of the fields arising in each measurement configuration is receiving a great deal of attention. With the dominance of the SBL method in the market, to date, the main focus has been biased toward analyzing the target's response at far source-receiver offsets of interest in the standard CSEM method. Furthermore, the problem is traditionally approached either by numerically simulating the response of realistic targets, or by semianalytically computing the fields observed in idealized 1D settings (Chave, 2009) as closed-form solutions are only possible to obtain for simplified

geometries. However, the closed-form solutions allow us to analyze the fundamental physics of the problem in a more compact way, leading to new insights of what a given technique has to offer. For instance, the seminal work of Baños (1966) (see also Bannister (1984)) describing the dipolar field in a two half-spaces system is used to study the properties of the so-called *airwave* component that masks the reservoir's response at large offsets in the standard CSEM configuration. The airwave phenomenon arises in the TE mode of the fields due to a HED excitation, thereby the VED time-domain measurement is ideally set up to avoid this effect. Concerning the three-media system, the work of Weidelt (2007) (as well as Loseth (2007)) described the theory introducing the concept of a *guided mode* of the EM fields appearing at long source-receiver offsets. Inside a resistive layer, the energy flow is channeled preferentially in the radial direction as it leaks out to the more conductive sur-

rounding. The formulas derived in Loseth (2007) show that at far offsets, the spatial falloff of the fields escaping the resistive channel follows an approximate $r^{1/2}e^{-i\lambda_0 r}$ dependence on the radial distance r, which dominates above the faster decaying primary field. The so-called *resistive layer pole* λ_0 depends on the resistivity-thickness product of the layer (Cuevas et al., 2009: Kong et al., 2010). From this observation, Kong et al. (2010) propose that estimates of the wavenumber in experimental data could be related to hydrocarbon indicators.

In the near-offset regime of the vertical source-receiver configuration the expressions derived in Loseth (2007) do not accurately describe the spatial falloff of the fields (see Loseth [2007] section §4.5.6). In fact, the contribution of the resistive layer pole diverges as approximately $\ln(\lambda_0 r)$ as $r \to 0$, and therefore, the role of the guided mode is not clear, or not present, at receiver locations close to the source. Loseth (2007) also includes terms of the form $|\omega\mu_0\sigma_1 r|^{-1}$ (e.g., equation 4.49 in Loseth (2007)) that improve the accuracy of the solution in the asymptotic regime of $|\omega\mu_0\sigma_1 r| \gg 1$. However, the inverse dependence on ω imposes a threshold frequency below that which the solution is not accurate, and therefore, it cannot be used to analyze the time-domain transient of the fields in which very low frequencies are required.

It is the purpose of this work to study the near-offset, spatial, and spectral distribution of the EM fields due to a VED or HED source located above a resistive layer inserted in an otherwise homogeneous whole-space (see Figure 2). The analysis is approached using closed-form solutions to provide basic understanding of the fields arising at near offsets in comparison to the long offset measurements. In particular, the analytical studies can explain the lack of sensitivity observed in near-offset measurements with an HED source and inline receiver, in comparison to the vertical source-receiver configuration. Moreover, closed-form solutions could reveal
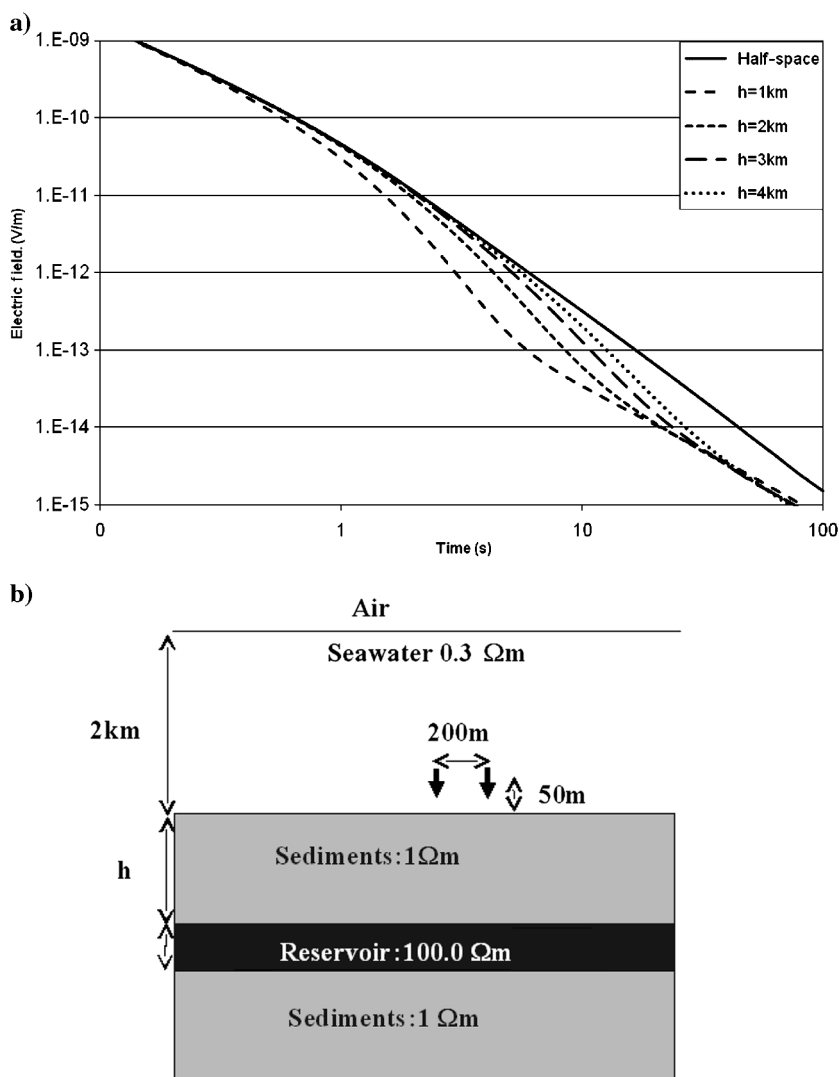

Figure 1. (a) Time-domain anomaly in the E_Z component due to the presence of a resistive layer, located at various depths ($h = 1, 2, 3,$ and 4 km) below the seafloor. (b) The model configuration consists of the resistive layer (100 Ω-m) that is inserted in 1 Ω-m sediments. The source and receiver are placed 50 m above the seafloor and their separation is fixed at 200 m.

hydrocarbon indicative properties of the fields, in analogy to those of the guided mode wave number, which have been exploited in Kong et al. (2010).

In the next section, a solution for the fields observed above the layer is established as a superposition of a direct and an image term, and a Fourier-Bessel integral in the complex wavenumber domain describing a secondary layer response. Asymptotic power series expansions of the fields are analyzed (Asymptotic solution 1 — High-frequency behavior section) in the high frequency regime of $|\omega\mu_0\sigma_1 h| \gg 1$. A low frequency solution is obtained via a *Kernel Modulation* technique (Asymptotic solution 2 — Low frequency and late time-domain transient decay section), which in turn, yields suitable expressions for the analysis of the time-domain transient decay. Concluding remarks are presented last.

SOURCE, IMAGE, AND SECONDARY LAYER RESPONSE

Consider the simplified model described in Figure 2. A harmonic, unit electric dipole source ($\mathbf{J} = \hat{u}Ids\delta(x)\delta(y)\delta(z+h)e^{i\omega t}$, $\hat{u} = \hat{z}, \hat{x}$ for a VED and HED, respectively) is located at a distance h above the resistive layer of conductivity σ_2 and thickness h_2, in a whole-space of conductivity σ_1. The origin of the coordinate system coincides with the top boundary of the layer, thus, the source is located at $z = -h$, and the observation point is defined coplanar with the source (i.e., $y = 0$) and located above the layer at $z < 0$ (then $h - z > 0$), and at a radial distance r ($= x$) from the source.

Here, the work of Ward and Hohmann (1988) is extended to formulate the boundary value problem, subject to suitable boundary conditions, for the fields arising in the specific 1D problem of the scenario described above. After a few algebraic steps, it is easy to show that the solution yields a superposition of a *direct field* (D) and two components that account for the layer response; an *image term* (I) and the *secondary fields* (S). The image term represents the contribution due to the charge density induced by the direct field on the upper plane of the layer, and the secondary fields represent the effect of the finite thickness of the layer. Formally,

$$E_z = E_z^{(D)} - E_z^{(I)} + \frac{Ids}{4\pi\sigma_1}\int_0^\infty \frac{2K_1}{K_1 + \hat{Z}_2}\frac{\lambda^3}{u_1}J_0(\lambda r)e^{-u_1(h-z)}\mathrm{d}\lambda,$$

$$E_x = E_x^{(D)} - E_x^{(I)} - \frac{Ids}{4\pi\sigma_1}\int_0^\infty \frac{2K_1}{K_1 + \hat{Z}_2}\lambda^2 J_1(\lambda r)e^{-u_1(h-z)}\mathrm{d}\lambda,$$

$$H_y = H_y^{(D)} - H_y^{(I)} + \frac{Ids}{4\pi}\int_0^\infty \frac{2K_1}{K_1 + \hat{Z}_2}\frac{\lambda^2}{u_1}J_1(\lambda r)e^{-u_1(h-z)}\mathrm{d}\lambda,$$

$$K_i = \frac{u_i}{\sigma_i + i\epsilon_i\omega},$$

$$\hat{Z}_2 = K_2\frac{K_3 + K_2\tanh(u_2 h_2)}{K_2 + K_3\tanh(u_2 h_2)},$$

$$u_i = \sqrt{\lambda^2 - k_i^2},\qquad\text{and}$$

$$k_i^2 = -i\sigma_i\omega\mu_0 \tag{1}$$

for a VED source; whereas for a HED source, the fields are given by

$$E_x = E_x^{(D)} - E_x^{(I)} + E_x^{(TM)} + E_x^{(TE)},$$

$$E_z = E_z^{(D)} - E_z^{(I)} + E_z^{(TM)} + E_z^{(TM)},$$

$$H_y = H_y^{(D)} - H_y^{(I)} + H_y^{(TM)} + H_y^{(TM)}, \tag{2}$$

where the secondary field has been decomposed into its TM and TE components, which are given as

$$E_x^{(TM)} = \frac{Ids}{4\pi\sigma_1}\int_0^\infty \frac{2_2\hat{Z}}{Z_1 + \hat{Z}_2}u_1 e^{-u_1(h-z)}\left(\frac{J_1(\lambda r)}{r} - \lambda J_0(\lambda r)\right)\mathrm{d}\lambda,$$

$$E_z^{(TM)} = \frac{Ids}{4\pi\sigma_1}\int_0^\infty \frac{2\hat{Z}_2}{Z_1 + \hat{Z}_2}e^{-u_1(h-z)}\lambda^2 J_0(\lambda r)\mathrm{d}\lambda,$$

$$H_y^{(TM)} = \frac{Ids}{4\pi}\int_0^\infty \frac{2\hat{Z}_2}{Z_1 + \hat{Z}_2}e^{-u_1(h-z)}\left(\frac{J_1(\lambda r)}{r} - \lambda J_0(\lambda r)\right)\mathrm{d}\lambda,$$

$$Z_i = \frac{u_i}{\sigma_i + i\epsilon_i\omega},\qquad\text{and}$$

$$\hat{Z}_2 = Z_2\frac{Z_3 + Z_2\tanh(u_2 h_2)}{Z_2 + Z_3\tanh(u_2 h_2)} \tag{3}$$

for the TM mode, and by

$$E_x^{(TE)} = \frac{Ids}{4\pi\sigma_1}\frac{k_1^2}{r}\int_0^\infty \frac{2Y_1}{Y_1 + \hat{Y}_2}\frac{e^{-u_1(h-z)}}{u_1}J_1(\lambda r)\mathrm{d}\lambda,$$

$$E_z^{(TE)} = 0,$$

$$H_y^{(TE)} = \frac{Ids}{4\pi}\frac{1}{r}\int_0^\infty \frac{2Y_1}{Y_1 + \hat{Y}_2}e^{-u_1(h-z)}J_1(\lambda r)\mathrm{d}\lambda,$$

$$Y_i = \frac{u_i}{i\mu_0\omega},\qquad\text{and}$$

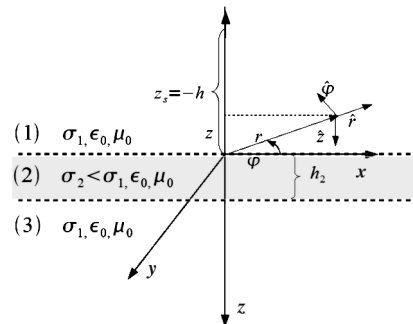$$\hat{Y}_2 = Y_2\frac{Y_3 + Y_2\tanh(u_2 h_2)}{Y_2 + Y_3\tanh(u_2 h_2)} \tag{4}$$

Figure 2. Three media configuration of the system of interest in this work. The resistive layer, of conductivity σ_2, and thickness h_2 is inserted in a homogeneous whole-space of conductivity $\sigma_1 > \sigma_2$. The origin of the coordinate system coincides with the top of the layer. Thus, $z > 0$ in the downward direction, the source is located at $z_s = -h$, and the observation point is defined for $z < 0$.

for the TE mode. By symmetry considerations, H_z vanishes identically at $y = 0$, i.e., for coplanar source-receiver positions. The integral representation of the secondary fields describes a superposition of plane waves of complex angle of incidence. The complex amplitude of the plane wave components is determined by matching boundary conditions for the fields observed at the upper and lower interfaces. The integration then accounts for that fraction of the energy that is transmitted through the layer and subsequently reflected at the lower interface.

The direct and image terms ($\mathbf{E}^{(D,I)}$ and $\mathbf{H}^{(D,I)}$) describe the fields arising from a dipole located above and below the plane of the upper interface, respectively, in a homogeneous whole-space of conductivity σ_1. Expressions for these components are readily available from equation 2.40 and equation 2.42 in Ward and Hohmann (1988) (for a HED excitation) or can be derived from such formulas by a suitable coordinate transformation (for a VED excitation). For completeness,

$$E_z^{(D,I)} = \frac{Ids}{4\pi\sigma_1} \frac{e^{-ik_1R}}{R^3} \left(r^2 k_1^2 - ik_1 R - 1 + \frac{3ik_1\Delta^2}{R} + \frac{3\Delta^2}{R^2} \right),$$

$$E_x^{(D,I)} = \frac{Ids}{4\pi\sigma_1} \frac{r\Delta e^{-ik_1R}}{R^3} \left(-k_1^2 + \frac{3ik_1}{R} + \frac{3}{R^2} \right),$$

$$H_y^{(D,I)} = -\frac{Ids}{4\pi} \frac{re^{-ik_1R}}{R^2} \left(ik_1 + \frac{1}{R} \right) \qquad (5)$$

for the VED excitation, and

$$E_z^{(D,I)} = \frac{Ids}{4\pi\sigma R^3} e^{-k_1R} \left[\frac{\Delta x}{R^2} (-k_1^2 R^2 + 3ik_1 R + 3) \right],$$

$$E_x^{(D,I)} = \frac{Ids}{4\pi\sigma R^3} e^{-k_1R} \left(\frac{x^2}{R^2} (-k_1^2 R^2 + 3ik_1 R + 3) \right.$$
$$\left. + (k_1^2 R^2 - ik_1 R - 1) \right),$$

$$H_y^{(D,I)} = -\frac{Ids}{4\pi R^2} e^{-k_1R} \left(\frac{\Delta}{R} (ik_1 R + 1) \right) \qquad (6)$$

for the HED excitation. The superscript (D, I) regards the *direct* or *image* component, such that $R = (x^2 + \Delta^2)^{1/2}$, with $\Delta = z + h$, $z - h$ for the direct (D) and image (I) components, respectively.

The secondary fields are derived after evaluating the Fourier-Bessel integrals in equations 1, 3, and 4. This is traditionally accomplished using a semianalytical approach, such as fast Hankel transform algorithms (e.g., Anderson (1979)). In what follows, the task is accomplished analytically for the system in which the resistive layer is embedded in homogeneous whole-space, such that $K_3 = K_1$, $Z_3 = Z_1$, and $Y_3 = Y_1$ on the integration kernels above.

ASYMPTOTIC SOLUTION 1 — HIGH FREQUENCY BEHAVIOR

Consider the behavior of the fields observed at close source-receiver offsets ($|k_1 r| \ll 1$), at high enough frequencies such that the skin depth in the overburden is much smaller than the vertical distance between the source and the layer ($|k_1(h - z)| \gg 1$). In this regime, the solutions for the secondary field integrals 1, 3, and 4 are well approximated by asymptotic series on $|k_1(h-z)|^{-1}$. The detailed derivation of the asymptotic series expansions of the fields is described in Appendix A, and the results are validated by comparison (e.g., Figure A-1 and Figure A-2) to semianalytical calculations of the fields (K. H. Lee, personal communication, 1988). The following approximated closed-form expressions are employed to interpret the structure of the fields in the near-offset regime of interest in this work.

For a VED excitation, the vertical component of the secondary field, $E_z^{(S)}$, can be approximated by equation A-24,

$$E_z^{(S)} \sim \frac{I_1 ds}{4\pi\sigma_1} \frac{e^{-ik_1(h-z)}}{(h-z)^3} 2[1 + ik_1(h-z) - 2n^2 ik_1 h_2]$$
$$- \frac{I_2 ds}{4\pi\sigma_1} \frac{e^{-ik_1(h-z)}}{(h-z)^3} 2[1 + ik_1(h-z) - 4n^2 ik_1 h_2]$$
$$I_1 = I,$$
$$I_2 = I \frac{ik_1 h_2}{2},$$
$$n^2 = \sigma_1/\sigma_2. \qquad (7)$$

On the other hand, using equation 5, the field due to a *biased image source*, i.e., a source located η m above the image at $z_s = h - \eta$, is approximated by

$$E_z^{(\eta)} \sim \frac{Ids}{4\pi\sigma_1} \frac{e^{-ik_1(h-z)}}{(h-z)^3} 2[1 + ik_1(h-z) - 2ik_1\eta], \qquad (8)$$

assuming that $(h - z) \gg \eta$ and $r \to 0$. Therefore, equation 7 describes the field arising due to a pair of such biased image sources, a source located at $\eta_1 = n^2 h_2$ and another one at $\eta_2 = 2n^2 h_2$. These image sources represent the cumulative effect of the charges induced at a given boundary by the field generated by the induced charge at the other boundary, and ultimately, the charge induced at the upper interface by the direct component. Furthermore, rearranging equation 7 to dominant order $O(k_1 h_2)$ and considering the near-offset approximation of the direct and image components (assuming $\Delta \ll r$ and $\Delta \gg r$ for the direct and image terms, respectively, in equation 5) yields the total field

$$E_z = E_z^{(D)} - E_z^{(I)} + E_z^{(S)},$$

$$E_z^{(D)} \sim \frac{Ids}{4\pi\sigma_1} \frac{e^{-ik_1 r}}{r^3} (r^2 k_1^2 - ik_1 r - 1),$$

$$E_z^{(I)} \sim \frac{Ids}{4\pi\sigma_1} \frac{e^{-ik_1(h-z)}}{(h-z)^3} 2[1 + ik_1(h-z)],$$

$$E_z^{(S)} \sim \frac{Ids}{4\pi\sigma_1} \frac{e^{-ik_1(h-z)}}{(h-z)^3} 2[1 + ik_1(h-z) - 2n^2 ik_1 h_2] - \dots \quad (9)$$

The secondary field,

$$E_z^{(S)} \sim E_z^{(I)} - \frac{Ids}{4\pi\sigma_1} \frac{e^{-ik_1(h-z)}}{(h-z)^3} (4n^2 ik_1 h_2) - \ldots, \qquad (10)$$

in part cancels the image term ($E_z^{(I)}$), suggesting that those sources induced on the upper boundary will induce a charge distribution in the lower boundary that is opposite in sign and therefore produces an opposing field. The remaining response of the layer is given by $4n^2 ik_1 h_2$ in equation 10, i.e., the secondary field depends on h_2/σ_2 or the resistive thickness product of the layer, a property that applies to the quasistatic behavior of the fields in the DC resistivity method (Kaufman (2010), Sharma (1997)).

Consider now the asymptotic solution for E_x, due to a HED. The field can be described as

$$E_x = E_x^{(D)} - E_x^{(I)} + \left[E_x^{(TM)} + E_x^{(TE)} \right], \qquad (11)$$

a superposition of a direct D and image I term, and the additional secondary layer response, contained in the TE and TM modes of the secondary fields (equation A-30 and equation A-42), which can be approximated as

$$E_x^{(TM)} = \frac{Ids}{4\pi\sigma_1} \frac{k_1^2}{(h-z)} e^{-ik_1(h-z)} \left[1 + \frac{1}{ik_1(h-z)} + \frac{1}{[ik_1(h-z)]^2} \right] - \frac{Ids}{4\pi\sigma_1} \frac{k_1^2}{2(h-z)} e^{-ik_1(h-z)} \left(1 - n^2 \frac{h_2}{(h-z)} + \frac{3in^2}{k_1} \frac{h_2}{(h-z)^2} \right) \qquad (12)$$

and

$$E_x^{(TE)} = \frac{Ids}{4\pi\sigma_1} \frac{k_1^2}{2(h-z)} e^{-ik_1(h-z)} \left[1 - \frac{h_2}{(h-z)} \left(\frac{1}{2} - \frac{\sigma_2}{\sigma_1} \right) \right] \qquad (13)$$

for the TM and TE modes, respectively. Similarly, the image component of the total field due to a HED ($E_x^{(I)}$ for $r \ll |h-z|$) is given by

$$E_x^{(I)} = \frac{Ids}{4\pi\sigma_1} \frac{k_1^2}{(h-z)} e^{-ik_1(h-z)} \left[1 + \frac{1}{ik_1(h-z)} + \frac{1}{(ik_1(h-z))^2} \right]. \qquad (14)$$

It is evident that the first term in equation 12 exactly opposes the image term in equation 14. The opposing image is obtained solely from the TM mode of the fields, as the TE field is continuous across the interface, and thereby, it does not induce a charge density at the layer boundaries. From a practical standpoint, it is noted that the layer response of the TE mode is contained in the expression $(h_2/(h-z))(\sigma_2/\sigma_1)$ of equation 13, which is negligible in comparison to unity (for $\sigma_2:\sigma_1 = 1:10$, and $h_2:(h-z) = 50:2000$, $(h_2\sigma_2)/(\sigma_1(h-z)) \sim O(10^{-3})$). This analytically shows the

empirically known fact that the fields described by the TE mode are rather insensitive to the properties of the layer.

The secondary layer response is left in the TM mode (equation 12) in as much as $n^2 h_2/(h-z)$ compares with unity (for $\sigma_2:\sigma_1 = 1:10$, and $h_2:(h-z) = 50:2000$, $n^2(h_2/(h-z)) \sim 0.25$). Indeed, replacing $n^2 = \sigma_1/\sigma_2$ in equation 12 shows that the remaining response of the layer is proportional to the resistivity-thickness product, and inversely with the source-receiver distance to the target. Swidinsky and Edwards (2009) demonstrate the lack of sensitivity of the TE mode in the response of 2D resistive targets, but the dependence on transverse impedance of the TM mode was assumed in the underlaying resistive thin sheet approximation of their solution. That is, they formulated the solution under the assumption that the layer's thickness is much smaller than its depth, and in that the response of the target depends on the resistivity-thickness product, rather than the individual properties.

ASYMPTOTIC SOLUTION 2 — LOW FREQUENCY AND LATE TIME-DOMAIN TRANSIENT DECAY

In practice, the behavior of the fields as a function of time depends on the nature of the source, in as much as the source time function differs from a pure harmonic excitation. Given the spectral content of the source $J_s(\omega)$, the time dependence of the resulting fields is obtained as a superposition of the spectral content of the fields (e.g., $E(\omega)$) weighted by the spectrum of the source, i.e., by the inverse Fourier transform

$$e(t) = \frac{1}{2\pi} \int_{-\infty}^{+\infty} E(\omega) J_s(\omega) e^{i\omega t} d\omega. \qquad (15)$$

For a *step on* (*step off*) time dependence of the source, it is well known that the spectral content is inversely proportional to frequency, i.e., $J_s(\omega) = 1/(i\omega)$, thereby the behavior of the fields at late times is strongly dependent on the spectrum of the fields at low frequencies. In this regard, the inverse dependence $(ik_1(h-z))^{-n}$ in equations A-15, A-17, and A-20 indicates that the formulas are accurate for short wavelengths in the conducting medium such that $|k_1(h-z)| \gg 1$. For a given source-layer distance $(h-z)$, a low-frequency threshold appears, below which the asymptotic solutions cannot accurately describe the behavior of the fields, and thereby cannot be inverted to derive the time-domain representation of the fields. To overcome this limitation, a Kernel modulation scheme is used to evaluate the integral of the secondary fields. In this method, the integration kernels in equations 1, 3, and 4 are modulated by a suitable function that allows to extend the path of integration to $-\infty$. In turn, the path is deformed to enclose the singularities due to the resistive layer pole and those resulting at the poles of the modulating function. The *method of residues* (Morse and Feshbach, 1953) is used to evaluate the integrals by superimposing the residues determined at the positions of the poles. The solution yields an infinite series representation that accurately describes the spectrum of the fields to very low frequencies. The detail derivations are presented in Appendix B. In the following, only the main results are revisited to interpret the structure of the fields and discuss the time-domain transient behavior.

Consider the vertical electric field component due to a VED excitation. The secondary field in the frequency domain is given by

$$E_z^{(S)} = \frac{Ids}{4\pi\sigma_1}(-i2\pi)\sum_{n=0}^{\infty}\left(\frac{K_1}{K_1+\hat{Z}_2}\right)_{\lambda=\lambda_n}\frac{\lambda_n^3 k_2}{u_{1n}}J_0(\lambda_n r)e^{-u_{1n}(h-z)}$$

$$\lambda_n = -ik_2(2n+1)\pi/2, \quad \text{for } n = 0, 1, 2, \ldots \quad (16)$$

In Figure 3, semianalytical calculation (symbols) are compared to the Kernel modulation results (solid lines) of equation 16, and the agreement is evident. However, simplifying assumptions are needed to interpret the behavior of the field. Henceforth, a regime of thick layer and high conductivity contrast such that $\sigma_2/\sigma_1 \gg |ik_1 h_2|$ is considered to obtain approximate expressions for the secondary fields in equation 16. In this case, equation 16 reduces to

$$E_z^{(S)} = \frac{Ids}{4\pi\sigma_1}\left(\frac{\pi^4\sigma_2^4}{8\sigma_1^4}\right)\sum_{n=0}^{\infty}(ik_1 p_n)^3 f_n e^{-ik_1(h-z)C_n},$$

$$f_n = \frac{ik_1 + \sigma_1/(\sigma_2 h_2)}{ik_1(C_n-1)+\sigma_2/(\sigma_1 h_2)}$$

$$+ \frac{ik_1 - \sigma_1/(\sigma_2 h_2)}{ik_1(C_n+1)+\sigma_2/(\sigma_1 h_2)},$$

$$p_n = 2n+1,$$

$$C_n = \left(1+\frac{p_n^2\pi^2\sigma_2}{4\sigma_1}\right)^{1/2}, \quad (17)$$

which is in very good agreement with semianalytical calculations (see Figure 4a). The limiting behavior of the infinite summation in 17 yields
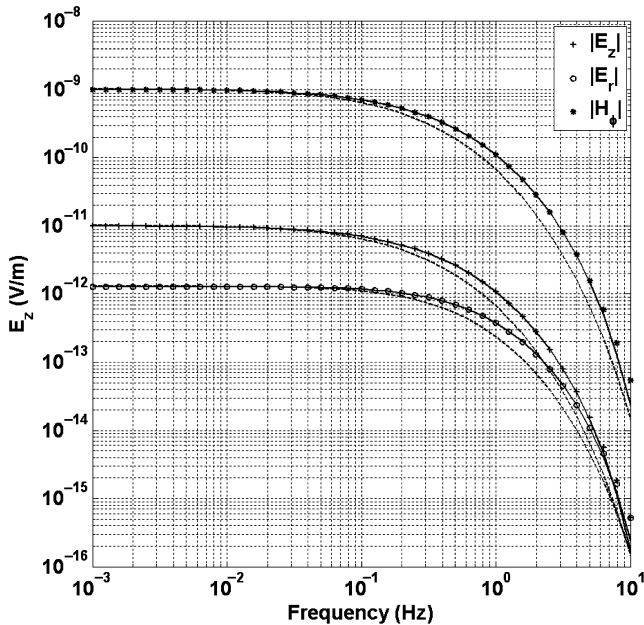

Figure 3. Layer response for $\sigma_1 : \sigma_2 = 50$ contrast, $h_2 = 30$ m, $h = |z| = 1$ km, and $r = 200$ m. Symbols depict semianalytical calculations and solid lines are obtained using equation B-1. Dashed lines show the results obtained the high-contrast, thin-layer $(\sigma_2/\sigma_1 \gg |ik_1 h_2|)$ approximation. The latter is accurate only in the low-frequencies regime.

$$\lim_{n\to\infty} E_z^{(S)} \sim \frac{I_{s1}ds}{4\pi\sigma_1}\frac{e^{-ik_1(h-z)}}{(h-z)^3}2\left[1+ik_1 h_2\frac{\sigma_2}{\sigma_1}\right]$$

$$-\frac{I_{s2}ds}{4\pi\sigma_1}\frac{e^{-ik_s(h-z)}}{(h-z)^3}2\left[1+ik_s(h-z)+\frac{1}{2}(ik_s(h-z))^2\right]$$

$$I_{s1} = I\frac{\pi^4}{16}\left(\frac{\sigma_2}{\sigma_1}\right)^2,$$

$$I_{s2} = I\pi^2\left(\frac{\sigma_2}{\sigma_1}\right)^3,$$

$$k_s = \frac{p_0\pi}{4}k_2, \quad (18)$$

which represents the familiar dipolar character of image sources at near offsets, already recognized in the previous section. The first term captures the effect of a biased image, but most importantly, the second term represents the fields due to an image source located in a whole-space medium which has the properties of the resistive layer ($k_s \propto k_2$), i.e., this field is associated with the charges induced in the lower boundary by the fields due to the charges in the upper boundary.

Time-domain expressions of the secondary fields (B-6, B-7, B-8, B-9, and B-10) are obtained from the inverse Fourier transform of equation 17, assuming a step on excitation. The time-domain behavior of the total field is obtained by superimposing that of the direct field, the image term, and secondary field, i.e.,

$$e_z(t) = e_z^{(D)} - e_z^{(I)} + e_z^{(S)}$$

$$e_z^{(D,I)}(t) = \frac{Ids}{4\pi\sigma_1 R^3}\left\{\left[\left(\frac{4}{\pi^{1/2}}\theta^3 R^3 + \frac{6}{\pi^{1/2}}\theta R\right)e^{-\theta^2 R^2}+3erfc(\theta R)\right]\frac{\Delta^2}{R^2}\right.$$

$$\left.-\left[\left(\frac{4}{\pi^{1/2}}\theta^3 R^3 + \frac{2}{\pi^{1/2}}\theta R\right)e^{-\theta^2 R^2}+erfc(\theta R)\right]\right\};$$

$$\theta = \left(\frac{\mu_0\sigma_1}{4t}\right)^{1/2}$$

$$e_z^{(S)} = e_z^{(A)} + e_z^{(B)}$$

$$e_z^{(A)} = \frac{Ids}{4\pi\sigma_1}\left(\frac{\pi^4\sigma_2^4}{8\sigma_1^4}\right)\sum_{n=0}^{\infty}E_n\left\{\frac{F_n}{\sqrt{\pi t}}e^{-\gamma_n^2/4t}-G_n e^{\alpha_n\gamma_n+\alpha_n^2 t}erfc\right.$$

$$\left.\left(\alpha_n\sqrt{t}+\frac{\gamma_n}{2\sqrt{t}}\right)\right\}. \quad (19)$$

Here, $R = (x^2+\Delta^2)^{1/2}$, and $\Delta = z+h, z-h$ for the direct and image components, respectively, and the coefficients F_n, G_n, E_n, α_n, and γ_n are described in equations B-7 and B-9. The expression for $e_z^{(B)}$ is obtained from $e_z^{(A)}$ after manipulating the coefficients as shown in equation B-9. The formulas in equation 19 are verified in Figure 4b, where the total field (solid line) is compared with semianalytical estimates (circles). The agreement is very good, thus validating the analysis that follows.

The behavior of the direct and image components is easy to see in Figure 4b. At late times, the contribution of the image term (in crosses) asymptotes and opposes that of the direct field, and thereby, the residual field is dominated by the secondary field. From a practical standpoint, this suggests that a time threshold could be defined beyond which the layer response begins to dominate. Indeed, assuming that $|h-z| \gg r$, the direct and image term asymptote $(e_z(t)^{(I)} \to e_z(t)^{(S)})$ at time t_0, such that

$$\frac{\mu_0 \sigma_1}{4t_0} = \frac{1}{(r^2 - (h-z)^2)} \ln\left(\frac{(h-z)^2}{2r^2}\right), \quad (20)$$

beyond which the decay of the direct and image fields behaves as $(\mu_0\sigma_1/4t)^{1/2}$.

The secondary fields ($e_z^{(S)}$), carrying the dependence of the layer's properties, can be interpreted as due to the superposition of an infinite number of biased image sources (Figure 5). Therefore, the time dependence in the summation on $e_z^{(A,B)}$ closely corresponds to that of the time-domain behavior of the field due to a vertical dipole in a homogeneous medium, excited by an exponential decay. This is given by a functional of the form (Wait, 1960)
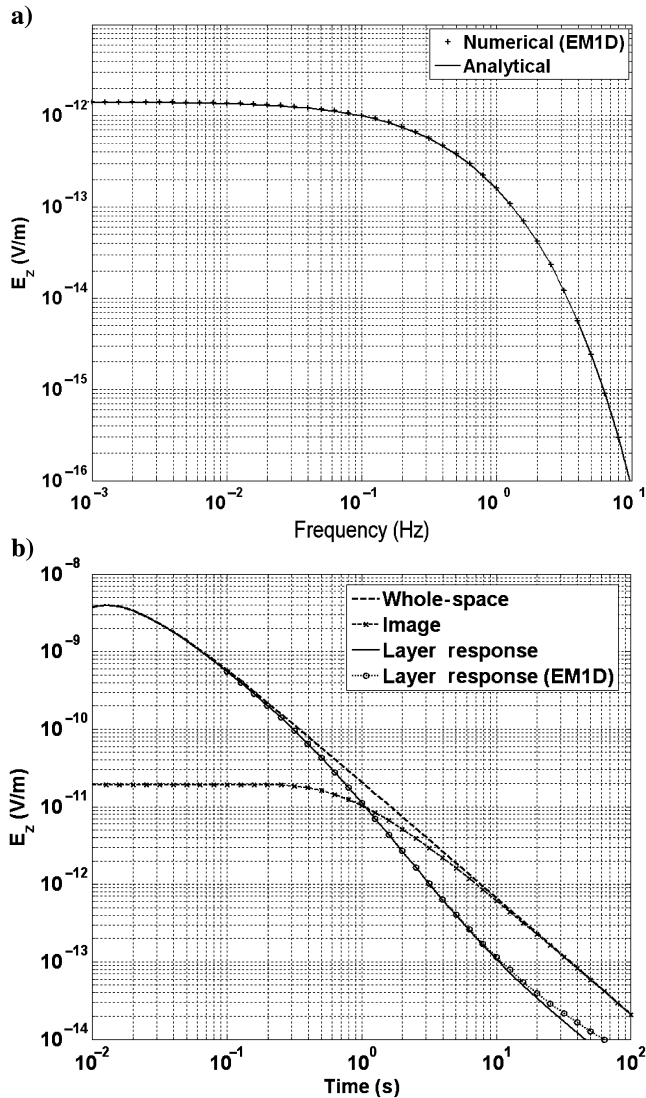
a)

Figure 4. (a) Frequency and (b) time-domain response of the resistive layer in the near-offset (250 m), high-contrast ($\sigma_2:\sigma_1 = 1:100$), and thick-layer ($h_2 = 250$ m) approximation. Vertical dipole source and receiver are located at $h = 1$ km above the layer. The reversed polarity of the image source opposes the direct field, thereby revealing the residual layer response.

$$A(\beta, t) = \frac{\alpha}{\sqrt{\pi t}} e^{-\alpha^2/4t}$$
$$+ e^{-\beta t + \alpha\sqrt{\beta}}\left(1 - \sqrt{\beta}\alpha\right)erfc\left(\frac{\alpha}{2\sqrt{t}} + \sqrt{\beta t}\right),$$
$$\alpha^2 = \sigma\mu_0 R, \quad (21)$$

where the excitation $I = I_0 e^{-\beta t}$, σ is the conductivity of the whole-space and R the source-receiver distance.

The first term in equation 21 controls the rise speed of the function, therefore, the maximum point in the curve can be computed by negating its first derivative with respect to time. Performing this calculation for $e_z^{(A)}$ in equation 19 yields the peak time

$$t_m = \mu_0\sigma_1(h-z)^2\left[1 + \left(\frac{\pi p_n}{2}\right)^2 \frac{\sigma_2}{\sigma_1}\right]. \quad (22)$$

For small values of p_n, the term in parentheses ~ 1, and thereby $t_m \sim \mu_0\sigma_1(h-z)^2$, but as p_n increases, $t_m \sim \mu_0\sigma_2[p_n(h-z)\pi/2]^2$. In other words, increasing n in the summation yields the contribution to the field due to dipole sources located farther below the layer (at a distance $= p_n(h-z)\pi/2$). Furthermore, equation 22 also shows that as n increases, the maximum response shifts from having a dependence on the background conductivity σ_1 to depending on that of the layer, i.e., the layer's response appears at a linearly increasing time.

The decay rate of the image source represents the diffusion speed of the charges induced at the boundaries, and ultimately drives the rate of decay of the field. Comparing the second terms of equation 21 and $e_z^{(A)}$ in equation 19 reveals that

$$\beta = \alpha_n^2 = \frac{1}{\mu_0\sigma_1}\frac{1}{[\sigma_1(C_n - 1)]^2}\left(\frac{\sigma_2}{h_2}\right)^2 \quad (23)$$
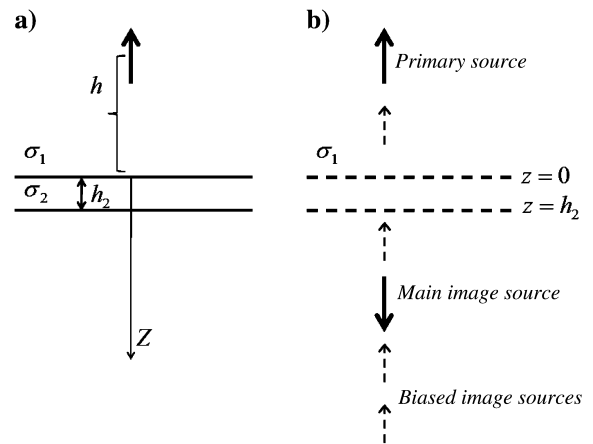
Figure 5. (a) The real system of a dipole in the presence of a resistive layer can be represented by (b) the fictitious problem of a dipole source and a superposition of dipolar image sources. The properties of the image sources (position and moment) are determined such that the boundary conditions of the real problem are satisfied by the fictitious problem. The solution to the boundary value problem yields a main image located below the upper interface (at $z = h$), and the superposition of secondary images which give rise to the secondary field.

is driven by the inverse of the resistivity-thickness product of the layer, i.e., the charges induced on the boundaries will diffuse slower for more resistive (or thicker) layers. This suggests that the diffusion of the boundary charge density is driven by conduction in the upper medium. Indeed, as the resistivity of the layer increases or as the layer thickens, the conduction path is dominated by the conductor above the layer. In this medium, the field decays slower, and thereby, it yields a slower decay rate for the charges induced at the boundary.

Consider now the fields due to a HED. The detailed derivation of the expressions describing the fields is presented in Appendix B. The following main results are summarized as required by the analysis. The total field

$$E_x = E_x^{(S)} - E_x^{(I)} + (E_x^{(TE)} + E_x^{(TM)}) \qquad (24)$$

comprises the direct (S) and layer response comprised of the image term (I), and the secondary layer response decomposed in the TE and TM modes. Each component can be approximately described as

$$E_x^{(I)} = \frac{Ids}{4\pi\sigma_1}\frac{k_1^2}{(h-z)}e^{-ik_1(h-z)}\left[1 + \frac{1}{ik_1(h-z)} + \frac{1}{(ik_1(h-z))^2}\right],$$

$$E_x^{(TE)} = \frac{Ids}{4\pi\sigma_1}\frac{k_1^2}{2(h-z)}e^{-ik_1(h-z)},$$

$$E_x^{(TM)} = \frac{Ids}{4\pi\sigma_1}\frac{k_1^2}{(h-z)}e^{-ik_1(h-z)}\left[1 + \frac{2}{ik_1(h-z)} + \frac{2}{[ik_1(h-z)]^2}\right]$$
$$+ E_x^{(TMS)}. \qquad (25)$$

The TE and TM expressions are in good agreement with semianalytical estimates (see Figure 6), thereby validating the analysis that follows.
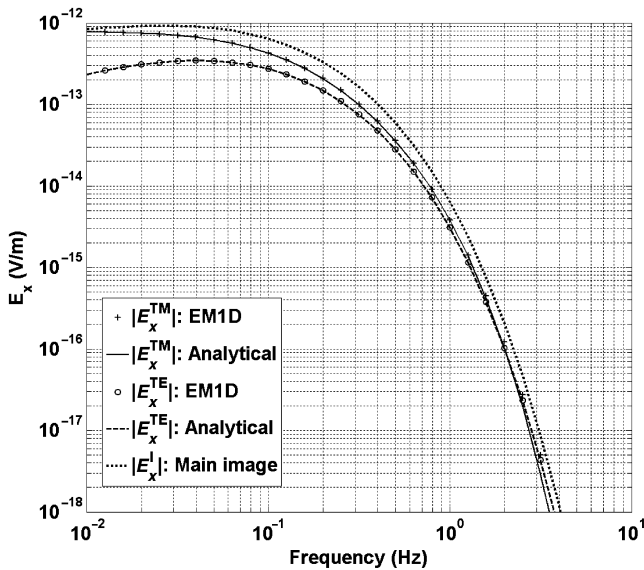

Figure 6. Comparison of analytical and semianalytical evaluation of the integrals. The model consists of a 20-m-thick, 40-Ωm layer, embedded in a 1-Ωm whole-space, and the HED source is located at $z_s = -h = 2500$ m.

The $E_x^{(TMS)}$ component is given by the infinite summation resulting from Kernel Modulation solution in equation B-17, i.e.,

$$E_x^{(TMS)} = \frac{Ids}{4\pi\sigma_1}(-2\pi i)\frac{k_2}{2}\sum_{n=0}^{\infty}\left(\frac{Z_1}{Z_1 + \hat{Z}_2}\right)_{\lambda=\lambda_n}\frac{\lambda_n^3}{u_{1n}}W_n e^{-u_{1n}(h-z)},$$

$$W_n = \left(1 - \frac{k_1^2}{\lambda_n^2}\right) = 1 + \frac{1}{p_n^2}\left(\frac{\sigma_1}{\sigma_2}\frac{4}{\pi^2}\right). \qquad (26)$$

As the summation index n increases, the pole λ_n increases, and in turn, the coefficient $W_n \to 1$. In this case, $E_x^{(TMS)} \to E_z^{(S)}$ of equation 16, i.e., the secondary TM response resembles that observed in the vertical source-receiver configuration.

The time-domain transient decay expressions of the fields are summarized by

$$e_x(t) = e_x^{(S)} - e_x^{(I)} + e_x^{(TE)} + e_x^{(TM)},$$

$$e_x^{(S)} = \frac{Ids}{4\pi\sigma_1}\frac{2}{r^3}\left(\frac{2\theta r}{\pi^{1/2}}e^{-\theta^2 r^2} - erfc(\theta r)\right),$$

$$\theta = \left(\frac{\mu_0\sigma_1}{4t}\right)^{1/2},$$

$$e_x^{(I)} = \frac{Ids}{4\pi\sigma_1}\frac{1}{(h-z)^3}\left\{\left(\frac{4\theta^3(h-z)^3}{\pi^{1/2}} + \frac{2\theta(h-z)}{\pi^{1/2}}\right)\right.$$
$$\left. e^{-\theta^2(h-z)^2} + erfc[\theta(h-z)]\right\},$$

$$e_x^{(TE)} = -\frac{Ids}{4\pi\sigma_1}\frac{1}{(h-z)^3}\left(\frac{2\theta^3(h-z)^3}{\pi^{1/2}}\right)e^{-\theta^2(h-z)^2},$$

$$e_x^{(TM)} = \frac{Ids}{4\pi\sigma_1}\frac{1}{(h-z)^3}\left\{\left(\frac{4\theta^3(h-z)^3}{\pi^{1/2}} + \frac{4\theta(h-z)}{\pi^{1/2}}\right)\right.$$
$$\left. e^{-\theta^2(h-z)^2} + 2erfc[\theta(h-z)]\right\} + e_x^{(TMS)}(t). \qquad (27)$$

The validity of the solution is established again by comparison of the total field with semianalytical estimates, as shown in Figure 7a.

The dominant contribution of the TM mode $E_x^{(TM)}$ partially opposes the image fields, thus the frequency spectrum of the scattered field is driven by the TE mode, which is independent of the layer's parameters. From a practical point of view, the final superposition that yields the total field yields a masked response of the layer, dominated by the direct field and TE mode, and thereby, insensitive to the properties of the layer.

In contrast to the late time behavior observed in the vertical source-receiver configuration (see. Figure 4b), in the horizontal source-receiver configuration, the superposition of the TM and TE secondary response opposes the contribution of the image term. In other words, the HED does not produce such an image field to oppose that of the direct component as observed in the vertical source-receiver configuration. Evidently, from Figure 7a, the overall behavior results in a dominating direct field, thereby explaining the lack of sensitivity to the properties of the layer.
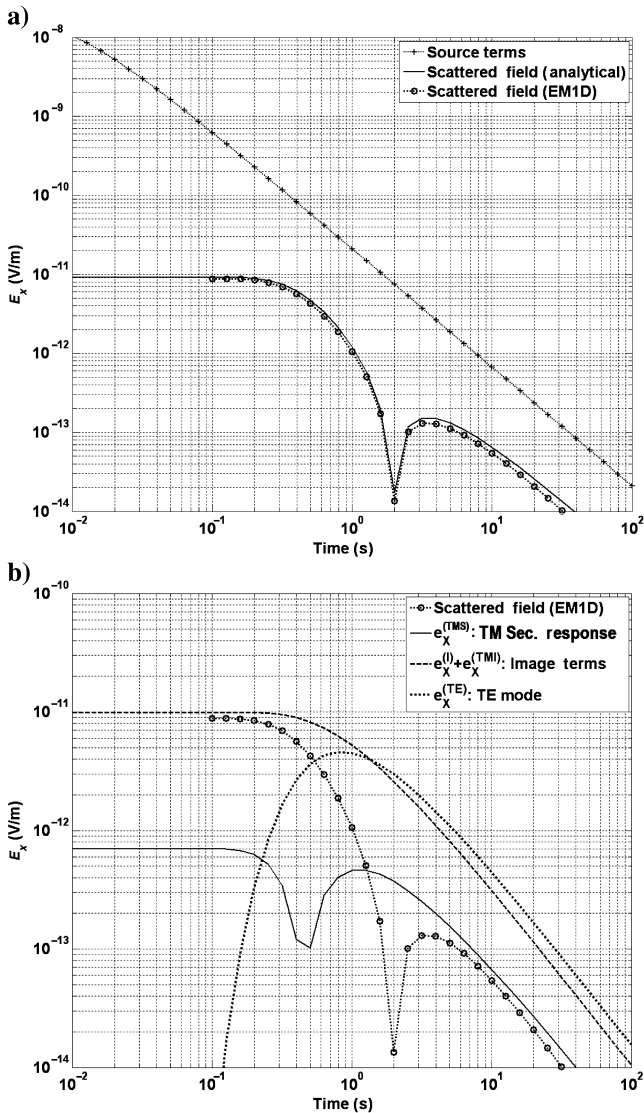
a)

b)

Figure 7. (a) Time-domain analytic solution in comparison to semi-analytical estimates of the scattered field (superposition of image, and secondary fields, TE, and TM) and (b) components of the scattered field solution 27. The curved labeled as $e_x^{(I)} + e_x^{(TMI)}$ corresponds to the superposition of the image term $e_x^{(I)}$ and the image like part of the TM field (first term of $e_x^{(TM)}$).

CONCLUSIONS

In this paper, we have derived expressions for the EM fields observed at near offsets from a vertical and horizontal electric dipole source located above a resistive layer. Different techniques have been applied to examine the behavior of the fields in frequency and time domain. Power series expansion of the fields in the frequency domain have been obtained using the saddle point method of integration. The formulas describing the fields are in good agreement when checked against semianalytical estimates of the frequency spectrum of the fields. However, the validity of the solution only holds for short wavelengths in the conducting medium, much shorter than the vertical distance to the source h, i.e., such

that $|k_1(h-z)| \gg 1$. As a consequence, the near DC behavior of the fields is not appropriately accounted for in the asymptotic expansion formulation. There is a lower bound for the frequency of applicability of this solution, and thereby, the time-domain inverse (Laplace transformed) of the asymptotic formulas will be biased for time scales longer than that of the threshold frequency. To overcome this limitation, a Kernel modulation scheme has been applied to evaluate the convolution integral to the lowest frequency required. The expressions obtained for the fields using this technique are in excellent agreement with the semianalytical calculation. The solution is approximated using a high-contrast, thick layer assumption which yields simplified expressions for the frequency spectrum and time-domain transient decay of the field, which in turn were used for the analytical study of the properties of the fields.

Regarding the structure of the fields in the near-offset regime, the solution for the VED and HED indicate that the fields behave remarkably different from those observed at far offsets. At near offsets, the field is better described as that due to a superposition of image sources, associated with the charges induced at the boundaries of the system, in contrast to the far offsets behavior which is described as a guided mode associated with preferential energy flow inside the layer and leakage toward the surrounding medium.

The transient decay of the fields due to each image source is the same as that of a dipole driven by an exponentially decaying source, with a decay constant that depends inversely on the resistivity-thickness product of the layer. This shows that the diffusion rate of the charges distributed on the layer boundaries decreases with increasing resistivity (or thickness) of the layer. The peak magnitude of the fields due to an image source appears at increasing times, for those image sources located farther from the layer. For the closer image sources, the peak amplitude of the resulting field will depend on the background conductivity, whereas for the distant image sources, the peak amplitude will depend predominantly on the properties of the layer. This explains the late time response expected for the effect of the layer. Image theory shows that the vertical position of each image source is associated with the horizontal spread of the charges density at the boundaries. In fact, the charge density represented by farther image sources decreases smoothly away from the vertical axis along the horizontal plane of the boundaries.

Regarding the VED excitation, it has been found that the late time response of the image term appears to cancel the direct field, thus providing the response of the layer described by the Kernel modulation solution. For a HED, the superimposed contributions of the TE and TM modes appear to reinforce the direct fields instead, thus masking the effect of the layer, which is also described by the Kernel modulation expression. The solution obtained by the Kernel modulation scheme allows to more clearly infer the contribution of the dipolar character of the charges induced in the lower boundary, and in passing, to verify that the concept of the superposition of images also holds in the low-frequency limit where the asymptotic solutions are not accurate enough.

As a last remark, it is important to notice that the expressions derived in this work have been oversimplified to render interpretable formulas, either by studying their limiting behavior, or by constraining the analysis based on the skin depth of the fields in the overburden, or the conductivity contrast in relation to the thickness of the layer. Therefore, caution must be exercised when using the derived expression in comparison to numerical estimates of the fields.

ACKNOWLEDGMENTS

APPENDIX A

ASYMPTOTIC REPRESENTATION

The half-saddle point method of integration described in Baños (1966) (§5) is used to evaluate the integrals in equations 1, 2, 3, and 4. In this scheme, a suitable conformal transformation ($\lambda \to x$) yields an expression of the form

$$e^{-ik_1(h-z)} \int_0^\infty \Phi(x) e^{-\frac{1}{2}x^2} \mathrm{d}x \tag{A-1}$$

for the Fourier-Bessel integrals equations 1, 2, 3, and 4. The function $\Phi(x)$ is a power series expanded version of the integration kernels, i.e.,

$$\Phi(x) \sim \sum_{m=0}^\infty A_{2m+1} x^{2m+1} \tag{A-2}$$

such that the integral is then evaluated term by term, using the formula

$$\int_0^\infty x^{2m+1} e^{-\frac{1}{2}x^2} \mathrm{d}x = 2^m m!. \tag{A-3}$$

SERIES EXPANSION — VED

Consider the fields due to the vertical electric dipole source (equation 1). In preparation for the integration in equation A-1, the integrands in each of equations 1, 2, 3, and 4are expanded in series of x so as to construct the function $\Phi(x)$. To this end, the transformation from $\lambda = k_1 \sin \alpha$ is first applied, such that in the alpha plane

$$u_1 = (\lambda^2 - k_1^2)^{1/2} = ik_1 \cos \alpha,$$
$$u_2 = (\lambda^2 - k_1^2)^{1/2} = i(k_2^2 - k_1^2 \sin^2 \alpha)^{1/2}. \tag{A-4}$$

The formulas

$$\xi = cx; \quad c = (-ik_1(h-z))^{-1/2}, \quad \cos \alpha = 1 - \frac{1}{2}\xi^2,$$
$$\sin \alpha = \xi\left(1 - \frac{1}{4}\xi^2\right)^{1/2}, \quad \sin \alpha \, d\alpha/dx = c\xi \tag{A-5}$$

are then used to attain the second transformation from $\alpha \to x$.

The small argument approximation $\tanh(u_2 h_2) \sim u_2 h_2$ is used to simplify the series expansion of

$$\frac{1}{K_1 + \tilde{Z_2}} = \sigma_1 \sigma_2 \left(\frac{u_2\sigma_1 + u_1\sigma_2 \tanh(u_2 h_2)}{2u_1 u_2 \sigma_1 \sigma_2 + \tanh(u_2 h_2)(u_1^2\sigma_2^2 + u_2^2\sigma_1^2)} \right)$$
$$\sim \sigma_1 \sigma_2 \left(\frac{\sigma_1 + u_1\sigma_2 h_2}{2u_1\sigma_1\sigma_2 + h_2(u_1^2\sigma_2^2 + u_2^2\sigma_1^2)} \right). \tag{A-6}$$

It could be argued that this approximation cannot be used due to the ∞ limit for the integration, as in fact $u_2 h_2 \to \infty$ as $\lambda \to \infty$ ($u_2^2 = \lambda^2 - k_2^2$), i.e., it diverges. However, as $|\lambda| \gg |k_1|$, $|k_2|$, $u_1 \sim \lambda$, $u_2 \sim \lambda$, in which case equation A-6 reduces to

$$\frac{1}{K_1 + \tilde{Z}_2} \sim \frac{\sigma_1}{2\lambda} \left[\frac{1 + \frac{\sigma_2}{\sigma_1} \tanh(u_2 h_2)}{1 + \frac{\sigma_1}{\sigma_2} \tanh(u_2 h_2)} \right] \tag{A-7}$$

where the denominator increases faster than the numerator, and therefore, the approximated integrand will converge regardless.

The expanded version of equation A-6 yields

$$\frac{1}{K_1 + \tilde{Z}_2} \sim \frac{N_0}{D_0} \left[\frac{1 + N_2\xi^2}{1 + D_2\xi^2 + D_4\xi^4 + \ldots} \right],$$
$$D_0 = -k_1^2\sigma_2^2 h_2 \left[1 + n^2\left(1 - \frac{2i}{k_1 h_2}\right) \right],$$
$$D_2 = \frac{k_1^2\sigma_2^2 h_2}{D_0} \left(1 + n^4 - \frac{in^2}{k_1 h_2}\right),$$
$$D_4 = -\frac{k_1^2\sigma_2^2 h_2}{4D_0}(1 + n^4),$$
$$N_0 = \sigma_1\sigma_2^2(n^2 + ik_1 h_2),$$
$$N_2 = -\frac{ik_1 h_2}{2(n^2 + ik_1 h_2)}, \tag{A-8}$$

where $n = k_1/k_2$ has been defined.

In the near-offset approximation of interest in this work, the small argument approximation (Abramowitz and Stegun, 1972) can be used to expand the Bessel function, such that

$$J_0(k_1 r \sin \alpha) \sim 1 + C_2\xi^2 + C_4\xi^4 + \ldots$$
$$C_2 = \frac{(ik_1 r)^2}{4},$$
$$C_4 = -\frac{(ik_1 r)^2}{64}(4 - (ik_1 r)^2) \tag{A-9}$$

for $k_1 r \sin \alpha \to 0$, i.e., where the magnitude of $J_0(k_1 r \sin \alpha)$ is the highest.

The series expansion of the Bessel function of the first order is also obtained from the small argument approximation (Abramowitz and Stegun, 1972, equation 9.1.10), and thereby, $J_1(k_1 r \sin \alpha)$ can be conveniently represented by

$$J_1(k_1 r \sin \alpha) = \frac{\lambda r}{2} j_1(\lambda r),$$
$$j_1(\lambda r) \sim 1 + c_2\xi^2 + c_4\xi^4 + \ldots$$
$$c_2 = \frac{(ik_1 r)^2}{8},$$
$$c_4 = -\frac{(ik_1 r)^2}{32}\left(4 - \frac{(ik_1 r)^2}{6}\right). \tag{A-10}$$

In preparation for completing the expansions required for the integrand of E_z, equation 1 is rewritten as an integral in x instead,

$$E_z^{(S)} = \frac{Ids}{4\pi\sigma} \frac{2}{\sigma_1} e^{-ik_1 a} \int_0^\infty \left[\frac{1}{K_1 + \hat{Z}_2} \lambda^3 J_0(\lambda r) \right] e^{-\frac{x^2}{2}} d\lambda, \quad \text{(A-11)}$$

where $a = h - z$. The integrand in brackets in equation A-11 is then written as

$$\Phi(x) = \frac{1}{K_1 + \hat{Z}_2} J_0(\lambda r)(\sin^2 \alpha \cos \alpha)(\sin \alpha d\alpha/dx)$$

$$\text{(A-12)}$$

and thus using equation A-9

$$J_0(\lambda r)(\sin^2 \alpha \cos \alpha)(\sin \alpha d\alpha/dx)$$
$$\sim c\xi^3(1 + P_2\xi^2 + P_4\xi^4 + \dots),$$
$$P_2 = \frac{(ik_1 r)^2}{4} - \frac{3}{4}$$
$$P_4 = \frac{1}{8} - \frac{(ik_1 r)^2}{4}\left(1 - \frac{(ik_1 r)^2}{16}\right), \quad \text{(A-13)}$$

which yields the expanded integrand

$$\Phi(x) = \frac{N_0}{D_0}(c^4 x^3 + F_2 c^6 x^5 + F_4 c^8 x^7 + \dots),$$
$$F_2 = Q_2 + P_2,$$
$$F_4 = Q_4 + P_4 + Q_2 P_2,$$
$$Q_2 = N_2 - D_2,$$
$$Q_4 = D_2^2 - D_4 - D_2 N_2. \quad \text{(A-14)}$$

Replacing A-14 and integrating term by term as shown in A-3 yields

$$E_z^{(S)} \sim \frac{Ids}{4\pi\sigma} \frac{e^{-ik_1 a}}{a^2}\left(\frac{4ik_1}{2 + ik_1 h_2}\right)\left(1 - \frac{4F_2}{ik_1 a} + \frac{24F_4}{(ik_1 a)^2}\right)$$

$$\text{(A-15)}$$

Continuing with E_r, equation A-10 is replaced in the corresponding integral of 1, which yields

$$E_x^{(S)} = -\frac{Ids}{4\pi\sigma} \frac{r}{\sigma_1} e^{-ik_1 a} \int_0^\infty \left[\frac{1}{K_1 + \hat{Z}_2} u_1 \lambda^3 j_1(\lambda r) \right] e^{-\frac{x^2}{2}} d\lambda.$$

$$\text{(A-16)}$$

Following the procedure outlined above for E_z the integration for E_r yields

$$E_x^{(S)} \sim -\frac{Ids}{4\pi\sigma} \frac{e^{-ik_1 a}}{a^2}\left(\frac{2rk_1^2}{2 + ik_1 h_2}\right)\left(1 - \frac{4F_2}{ik_1 a} + \frac{24F_4}{(ik_1 a)^2}\right),$$

$$\text{(A-17)}$$

where the F_i coefficients are computed as in equation A-14, using the expressions for Q_i as in equation A-14, but with the P_i coefficients determined from the expansion of the integrand in brackets in equation A-16 instead, i.e.,

$$j_1(\lambda r)(\cos^2 \alpha \sin^2 \alpha)(\sin \alpha d\alpha/dx)$$
$$\sim c\xi^3(1 + P_2\xi^2 + P_4\xi^4 + \dots),$$
$$P_2 = \frac{(ik_1 r)^2}{8} - \frac{5}{4}$$
$$P_4 = \frac{1}{2} - \frac{6(ik_1 r)^2}{32}\left(1 - \frac{(ik_1 r)^2}{36}\right). \quad \text{(A-18)}$$

Similarly, the expression for the azimuthal component of the magnetic fields can be manipulated to yield,

$$H_y^{(S)} = \frac{Ids}{4\pi} \frac{r}{\sigma_1} e^{-ik_1 a} \int_0^\infty \left[\frac{1}{K_1 + \hat{Z}_2} \lambda^3 j_1(\lambda r) \right] e^{-\frac{x^2}{2}} d\lambda, \quad \text{(A-19)}$$

which results in the asymptotic series

$$H_y^{(S)} \sim \frac{Ids}{4\pi} \frac{e^{-ik_1 a}}{a^2}\left(\frac{2rk_1}{2 + ik_1 h_2}\right)\left(1 - \frac{4F_2}{ik_1 a} + \frac{24F_4}{(ik_1 a)^2}\right).$$

$$\text{(A-20)}$$

Again, the F_i coefficients are determined by equation A-14, with the P_i coefficients given by

$$P_2 = \frac{(ik_1 r)^2}{8} - \frac{3}{4}$$
$$P_4 = \frac{1}{8} - \frac{(ik_1 r)^2}{8}\left(1 - \frac{(ik_1 r)^2}{24}\right). \quad \text{(A-21)}$$

As given by equations A-15, A-17, and A-20, the closed-form solutions are in good agreement with the semianalytical estimates. However, it is admitted that the asymptotic expressions hold best under high-frequency assumptions ($|k_1(h - z)| \gg 1$) and with the requirement of small layer perturbation ($h \gg h_2$), such as those described in Figure A-1. Under these conditions, equation A-15 is suitable to analyze the structure of the fields in the near-offset approximation, of the vertical source-receiver configuration. However, to better understand the structure of the fields, the expansion coefficients in equation A-15 are further approximated to dominant order in $O[(ik_1 h_2)^2]$ and $O[(ik_1 r)^2]$. To this end, consider the expressions for F_2 and F_4 in equation A-14 for the E_z component,

$$F_2 \sim -\frac{1}{4}[1 - 2n^2 ik_1 h_2 + n^2(ik_1 h_2)^2 - \frac{n^2}{2}(ik_1 h_2)^3 + \dots - (ik_1 r)^2],$$

$$F_4 \sim -\frac{ik_1 h_2}{16}\Big[1 - 4n^4 ik_1 h_2 + 4n^4(ik_1 h_2)^2 - \frac{15n^2}{4}(ik_1 h_2)^3 + \dots$$
$$+ (ik_1 r)^2\left(\frac{2}{ik_1 h_2} - 2n^2 + 1 + n^2 ik_1 h_2 - \frac{n^2}{2}(ik_1 h_2)^2\right)\Big], \quad \text{(A-22)}$$

where $n^2 = \sigma_1/\sigma_2 \gg 1$ ($n^2 = 30$ for the example in Figure A-1). Keeping dominant terms, replacing the approximated coefficients in equation A-15, yields

$$E_z^{(S)} \sim \frac{Ids}{4\pi\sigma_1} \frac{e^{-ik_1 a}}{a^3}\left(\frac{4}{ik_1 h_2 + 2}\right)\Big[1 + ik_1 a - 2n^2 ik_1 h_2 - (ik_1 r)^2$$
$$- \frac{3}{2}\frac{h_2}{a}\left(1 - 4n^4 ik_1 h_2 + 2ik_1 r\left(\frac{r}{h_2}\right)\right)\Big], \quad \text{(A-23)}$$

where $a = h - z$. In addition, assuming that $h_2 \ll (h - z)$, and regarding $r \sim h_2$, but $r \ll 2^{1/2} h_2 \sigma_1 / \sigma_2$, equation A-23 can be further approximated as

$$E_z^{(S)} \sim \frac{I_1 ds}{4\pi\sigma_1} \frac{e^{-ik_1(h-z)}}{(h-z)^3} 2[1 + ik_1(h-z) - 2n^2 ik_1 h_2]$$
$$- \frac{I_2 ds}{4\pi\sigma_1} \frac{e^{-ik_1(h-z)}}{(h-z)^3} 2[1 + ik_1(h-z) - 4n^2 ik_1 h_2]$$
$$I_1 = I,$$
$$I_2 = I \frac{ik_1 h_2}{2}, \tag{A-24}$$

which renders a more amenable expression for the analysis.

SERIES EXPANSION — HED TM MODE

Consider now the TM component of the fields due to the horizontal electric dipole source. Using approximation $\tanh(u_2 h_2) \sim u_2 h_2$, the integration kernel in equation 3 can be written as

$$\frac{\hat{Z}_2}{Z_1 + \hat{Z}_2} \sim \sigma_1 \left[\frac{u_1\sigma_2 + u_2^2\sigma_1 h_2}{2u_1\sigma_1\sigma_2 + h_2(u_1^2\sigma_2^2 + u_2^2\sigma_1^2)} \right], \tag{A-25}$$
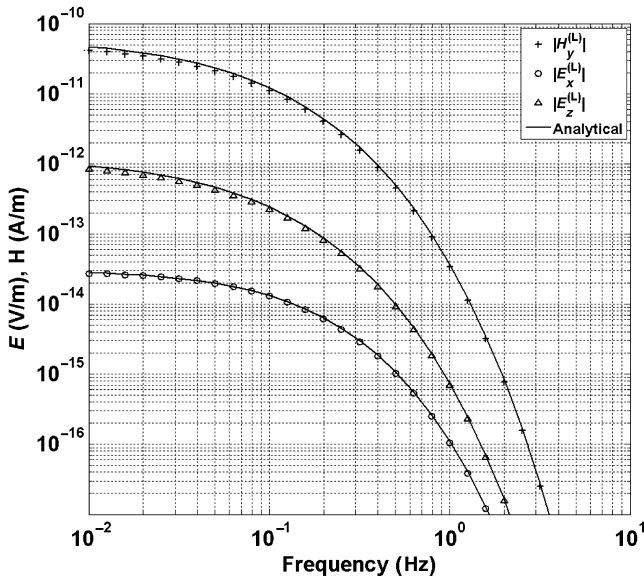
which expands to

Figure A-1. Fields observed above the layer at $r = 100$, $z = -h = -2.5$ km, due to a VED source. The resistive layer is $h_2 = 30$ m, and $\rho_2 = 30$ Ωm, and the background resistivity is $\rho_1 = 1$ Ωm. The symbols are then obtained using a semianalytical evaluation of the Bessel convolution integral (Anderson, 1979).

$$D = 2u_1\sigma_1\sigma_2 + h_2(u_1^2\sigma_2^2 + u_2^2\sigma_1^2),$$
$$D(\xi) = D_0(1 + D_2\xi^2 + D_4\xi^4),$$
$$D_0 = -k_1^2\sigma_2^2 h_2 \left[1 + n^2 \left(1 - \frac{2i}{k_1 h_2} \right) \right],$$
$$D_2 = -\left(\frac{1 + n^4 - in^2/(k_1 h_2)}{1 + n^2 - 2in^2/(k_1 h_2)} \right),$$
$$D_4 = \frac{1 + n^4}{4[1 + n^2 - 2in^2/(k_1 h_2)]} \tag{A-26}$$

for the denominator,

$$N = u_1\sigma_2 + u_2^2\sigma_1 h_2,$$
$$N(\xi) = N_0(1 + N_2\xi^2 + N_4\xi^4),$$
$$N_0 = ik_1\sigma_1\sigma_2(1 + ik_1 h_2),$$
$$N_2 = -\frac{1}{2} \left(\frac{1 + 2ik_1 h_2 n^2}{1 + ik_1 h_2} \right),$$
$$N_4 = \frac{ik_1 h_2 n^2}{4(1 + ik_1 h_2)} \tag{A-27}$$

for the numerator, and the Q_i coefficients are evaluated using equation A-14. As before, the expression for the fields are rewritten as

$$E_x^{(TM)} = \frac{Ids}{4\pi\sigma_1} \int_0^\infty \frac{2\hat{Z}_2}{Z_1 + \hat{Z}_2} \left[\left(\frac{1}{2}j_1 - J_0 \right) \cos^2\alpha \, \sin\alpha(d\alpha/dx) \right]$$
$$e^{-\frac{1}{2}x^2} dx, \tag{A-28}$$

and the expression in brackets expanded as

$$P(\xi) = \left(\frac{1}{2}j_1 - J_0 \right) \cos^2\alpha \, \sin\alpha(d\alpha/dx)$$
$$= -\frac{1}{2} c\xi(1 + P_2\xi^2 + P_4\xi^4 + \dots),$$
$$P_2 = -1 + \frac{3}{8}(ik_1 r)^2,$$
$$P_4 = \frac{1}{4} - \frac{(ik_1 r)^2}{32} \left(15 - \frac{5}{6}(ik_1 r)^2 \right),$$
$$P_6 = \frac{(ik_1 r)^2}{32} \left(6 - \frac{5}{6}(ik_1 r)^2 \right). \tag{A-29}$$

Replacing equations A-26 and A-27 yields

$$E_x^{(TM)} \sim \frac{Ids}{4\pi\sigma_1} \left(\frac{1 + ik_1 h_2}{2 + ik_1 h_2} \right) \frac{k_1^2}{a} e^{-ik_1 a}$$
$$\left[1 - \frac{2F_2}{ik_1 a} + \frac{8F_4}{(ik_1 a)^2} - \dots \right], \tag{A-30}$$

where the F_i coefficients are evaluated as inequation A-14.

Similarly $E_z^{(TM)}$ can be manipulated to yield,

$$E_z^{(TM)} = \frac{Ids}{4\pi\sigma_1} k_1^4 r e^{-ik_1 a}$$

$$\int_0^\infty \frac{\hat{Z}_2}{Z_1 + \hat{Z}_2} [j_1(\lambda r)\sin^2\alpha \cos\alpha(\sin\alpha d\alpha/dx)]e^{-\frac{1}{2}x^2}dx, \quad \text{(A-31)}$$

and the expression in brackets is expanded to

$$P(\xi) = j_1(\lambda r)\sin^2\alpha \cos\alpha(\sin\alpha d\alpha/dx)$$

$$= c\xi^3(1 + P_2\xi^2 + P_4\xi^4),$$

$$P_2 = -\frac{3}{4} + \frac{(ik_1 r)^2}{8}$$

$$P_4 = \frac{1}{8} - \frac{(ik_1 r)^2}{32}\left(7 - \frac{(ik_1 r)^2}{6}\right), \quad \text{(A-32)}$$

which yields

$$E_z^{(TM)} \sim -\frac{Ids}{4\pi\sigma_1}\left(\frac{1 + ik_1 h_2}{2 + ik_1 h_2}\right)\frac{2k_1^2 r}{a^2}$$

$$e^{-ik_1 a}\left[1 - \frac{4F_2}{ik_1 a} + \frac{24F_4}{(ik_1 a)^2} - \dots\right], \quad \text{(A-33)}$$

where the F_i coefficients are given by equation A-14, and P_i given by equation A-32.

The $H_y^{(TM)}$ is rewritten

$$H_y^{(TM)} = \frac{Ids}{4\pi}k_1^2 e^{-ik_1 a}\int_0^\infty \frac{2\hat{Z}_2}{Z_1 + \hat{Z}_2}\left[\left(\frac{1}{2}j_1 - J_0\right)\cos\alpha\sin\alpha(d\alpha/dx)\right]$$

$$e^{-\frac{1}{2}x^2}dx, \quad \text{(A-34)}$$

and now the expression in brackets is expanded to

$$P(\xi) = \left(\frac{1}{2}j_1 - J_0\right)\cos\alpha\sin\alpha(d\alpha/dx)$$

$$= -\frac{1}{2}c\xi(1 + P_2\xi^2 + P_4\xi^4),$$

$$P_2 = -\frac{1}{2} + \frac{3}{8}(ik_1 r)^2,$$

$$P_4 = -\frac{(ik_1 r)^2}{32}\left(9 - \frac{5}{6}(ik_1 r)^2\right), \quad \text{(A-35)}$$

which yields

$$H_y^{(TM)} \sim -i\frac{Ids}{4\pi}\left(\frac{1 + ik_1 h_2}{2 + ik_1 h_2}\right)\frac{k_1}{a}$$

$$e^{-ik_1 a}\left[1 - \frac{2F_2}{ik_1 a} + \frac{8F_4}{(ik_1 a)^2} - \dots\right], \quad \text{(A-36)}$$

where the F_i coefficients are given by equation A-14, with P_i given by equation A-35 instead.

SERIES EXPANSION — HED TE MODE

Consider now the TE component of the fields due to the horizontal electric dipole source. Using the approximation $\tanh(u_2 h_2) \sim u_2 h_2$, the integration kernel in equation 4 yields

$$\frac{1}{i\mu_0\omega}\frac{1}{Y_1 + \hat{Y}_2} \sim \frac{1 + u_1 h_2}{2u_1 + h_2(u_1^2 + u_2^2)}, \quad \text{(A-37)}$$

which when expanded provides

$$D = 2u_1 + h_2(u_1^2 + u_2^2),$$

$$D(\xi) = D_0(1 + D_2\xi^2 + D_4\xi^4),$$

$$D_0 = 2ik_1 - h_2 k_1^2(1 + n^{-2}),$$

$$D_2 = -\frac{1 + 2ik_1 h_2}{2 + ik_1 h_2(1 + n^{-2})},$$

$$D_4 = \frac{ik_1 h_2}{2 + ik_1 h_2(1 + n^{-2})} \quad \text{(A-38)}$$

for the denominator, and

$$N = 1 + u_1 h_2 = N_0(1 + N_2\xi^2),$$

$$N_0 = 1 + ik_1 h_2$$

$$N_2 = -\frac{ik_1 h_2}{2(1 + ik_1 h_2)} \quad \text{(A-39)}$$

for the numerator. The Q_i coefficients are evaluated using equation A-14. Following the same procedure, $E_x^{(TE)}$ in equation 4 is rewritten as

$$E_x^{(TE)} = \frac{Ids}{4\pi\sigma_1}k_1^4 e^{-ik_1 a}$$

$$\int_0^\infty \frac{1}{i\mu_0\omega}\frac{1}{Y_1 + \hat{Y}_2}[j_1 \cos\alpha\sin\alpha(d\alpha/dx)]e^{-\frac{1}{2}x^2}dx. \quad \text{(A-40)}$$

The expression in brackets is expanded to

$$P(\xi) = j_1 \cos\alpha\sin\alpha(d\alpha/dx)$$

$$= c\xi(1 + P_2\xi^2 + P_4\xi^4),$$

$$P_2 = -\frac{1}{2} + \frac{1}{8}(ik_1 r)^2,$$

$$P_4 = -\frac{(ik_1 r)^2}{32}\left(3 - \frac{1}{6}(ik_1 r)^2\right),$$

$$P_6 = -\frac{(ik_1 r)^2}{64}\left(1 - \frac{1}{6}(ik_1 r)^2\right), \quad \text{(A-41)}$$

which yields the expression for the fields

$$E_x^{(TE)} \sim \frac{Ids}{4\pi\sigma_1}\left(\frac{1 + ik_1 h_2}{2 + ik_1 h_2}\right)\frac{k_1^2}{a}$$

$$e^{-ik_1 a}\left[1 - \frac{2F_2}{ik_1 a} + \frac{8F_4}{(ik_1 a)^2} - \dots\right]. \quad \text{(A-42)}$$

The F_i coefficients are given by equation A-14, with P_i given by equation A-41.

The $E_z^{(TE)}$ component vanishes identically on the *TE* mode. The $H_y^{(TE)}$ component is rewritten as

$$H_y^{(TE)} = \frac{Ids}{4\pi} k_1^3 e^{-ik_1 a}$$

$$\int_0^{\infty} \frac{1}{i\mu_0\omega} \frac{1}{Y_1 + \hat{Y}_2} [j_1\cos^2\alpha \, \sin\,\alpha(d\alpha/dx)]e^{-\frac{1}{2}x^2} dx. \quad \text{(A-43)}$$

The expression in brackets is expanded to

$$P(\xi) = j_1 \cos^2\alpha \, \sin\,\alpha(d\alpha/dx)$$

$$= c\xi(1 + P_2\xi^2 + P_4\xi^4),$$

$$P_2 = -1 + \frac{1}{8}(ik_1 r)^2,$$

$$P_4 = \frac{1}{4} - \frac{(ik_1 r)^2}{32}\left(5 - \frac{1}{6}(ik_1 r)^2\right), \quad \text{(A-44)}$$

which yields this expression for the field

$$H_y^{(TE)} = \frac{Ids}{4\pi}\left(\frac{1 + ik_1 h_2}{2 + ik_1 h_2}\right)\frac{k_1}{a}$$

$$e^{-ik_1 a}\left[1 - \frac{2F_2}{ik_1 a} + \frac{8F_4}{(ik_1 a)^2} - \dots\right]. \quad \text{(A-45)}$$

The F_i coefficients are given by equation A-14, with P_i given by equation A-44.

As given by equations A-30, A-42, A-36, A-45, and A-33, the closed-form solutions are in very good agreement with the semia-
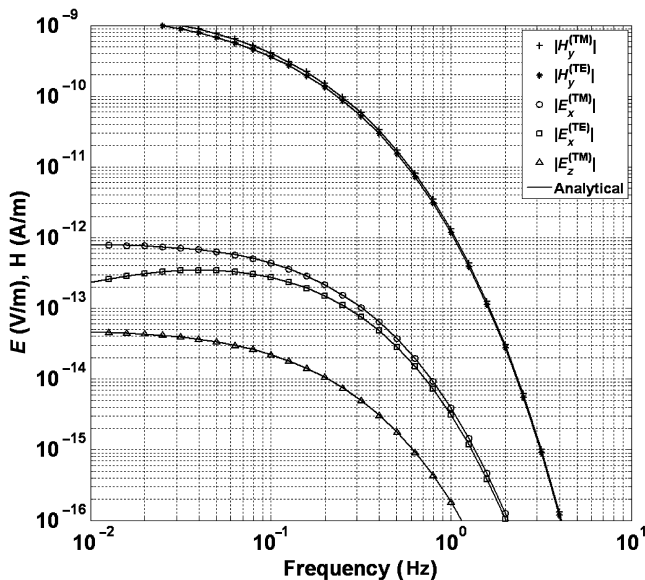

Figure A-2. Fields observed above the layer at $r = 100$, $z_s = -h = -2.5$ km, due to a HED source. The resistive layer is $h_2 = 30$ m, and $\rho_2 = 30$ Ωm, and the background resistivity is $\rho_1 = 1$ Ωm. The symbols are then obtained by semianalytical evaluation of the Bessel convolution.

nalytical estimates (Figure A-2), and thereby, they are suitable to analyze the structure of the fields in the near-offset approximation.

APPENDIX B

KERNEL MODULATION SOLUTION

To introduce the technique consider for instance the integration leading to the layer response in the vertical component E_z in equation 1. The integrand is an odd function of λ and thereby extending the limits to $-\infty$ amounts to zero after integration. The usual trick is to transform the integral to a Hankel convolution (Baños, 1966), then extend the limits to $-\infty$, and add the contribution of the resistive pole's residue to that around the branch points of the kernel at k_1 and k_2. However, it has been already pointed out that this solution diverges in the vicinity of the source, due to the singular behavior of $H_0^{(1)}(\lambda r \to 0)$.

In reference to Figure B-1, let I represent the integral from $0 \to \infty$ over the real axis of λ (path Γ_a), as defined in any of the expressions in equation 1. As the integrand is odd, the integral from $-\infty \to 0$ (path Γ_b) is $-I$, and also the integral from $0 \to -i\infty$ (path Γ_c) is I (as there are no singularities in the lower-left quadrant). It follows that the contribution from the pole's residue (at λ_0) plus that around the branch points (path Γ_d) is equal to that evaluated through $-\Gamma_c + \Gamma_a$, which is obviously zero.

The method of kernel modulation consists of multiplying the integral's kernel by a modulating function $m(\lambda) = \tanh(\lambda/k_2)$. This function does not modify significantly the kernel for those λs of greater weight (as the unperturbed kernel tends to zero very rapidly as $\lambda \to 0$), but it does invert the kernel for the negative λs, thereby making it even, and allowing to extend the limits to $-\infty$.

In the modulated integral, the contribution along the path Γ_d and the residue at the pole λ_0 do not vanish, but they can be neglected if the small perturbation assumption for the modulating function holds. In this case, the modulated integral can be evaluated approximately from the residues at the poles of the modulating function alone. These poles are located at $\lambda_n = -ik_2(2n+1)\pi/2$ for $n = 0, 1, 2, \dots$ (see Figure B-2), and the superposition of the residues of a given kernel at the position of each pole (Morse and Feshbach, 1953) yields the expressions for the fields.

SOLUTION FOR A VED EXCITATION

Applying the scheme above to the expressions in 1 yields

$$E_z^{(S)} = \frac{Ids}{4\pi\sigma_1}(-i2\pi)\sum_{n=0}^{\infty}\left(\frac{K_1}{K_1 + \hat{Z}_2}\right)_{\lambda=\lambda_n}\frac{\lambda_n^3 k_2}{u_{1n}}J_0(\lambda_n r)e^{-u_{1n}(h-z)},$$

$$E_x^{(S)} = -\frac{Ids}{4\pi\sigma_1}(-i2\pi)\sum_{n=0}^{\infty}\left(\frac{K_1}{K_1 + \hat{Z}_2}\right)_{\lambda=\lambda_n}\lambda_n^2 k_2 J_1(\lambda_n r)e^{-u_{1n}(h-z)},$$

$$H_y^{(S)} = \frac{Ids}{4\pi}(-i2\pi)\sum_{n=0}^{\infty}\left(\frac{K_1}{K_1 + \hat{Z}_2}\right)_{\lambda=\lambda_n}\frac{\lambda_n^2 k_2}{u_{1n}}J_1(\lambda_n r)e^{-u_{1n}(h-z)}, \quad \text{(B-1)}$$

where $u_{1n}^2 = \lambda_n^2 - k_1^2$. These expressions are in excellent agreement with semianalytical evaluation of the convolution integrals, as it is evident by comparing the solid lines versus the symbols in Figure 3. It is important to notice that the expressions in equation B-1 will render accurate estimates to whatever desired low-frequencies limit, depending only on the number of harmonics included in the summation (typically $n > 100$). However, further simplification is

needed to obtain expressions that are better suited to interpret the behavior of the fields.

Using equation A-6, it is easy to show that

$$\frac{1}{K_1 + \hat{Z}_2} \sim \frac{\sigma_1 \sigma_2}{h_2(\sigma_1^2 + \sigma_2^2)}\left(\frac{A}{u_{1n} - \alpha_1} + \frac{B}{u_{1n} - \alpha_2}\right),$$

$$A = -\left(\frac{\alpha_1 \sigma_2 h_2}{\alpha_2 - \alpha_1}\right),$$

$$B = \frac{\alpha_2 \sigma_2 h_2}{\alpha_2 - \alpha_1},$$

$$\alpha_{1,2} = \frac{1}{h_2}\left[-\frac{\sigma_2}{\sigma_1} \pm \left(\frac{\sigma_2^2}{\sigma_1^2} - h_2^2 k_1^2\right)\right]^{1/2}. \quad \text{(B-2)}$$

This equation can be further simplified under suitable approximations for the frequency range and model's properties. For example, a high-contrast and thin-layer approximation $(\sigma_2/\sigma_1 \gg |ik_1 h_2|)$ renders very simple expressions for the fields. However, this approximation is only useful at very low frequencies (dashed lines in Figure 3), and thereby, it cannot be used to obtain a time-domain representation. In what follows, a high-contrast, thick-layer approximation is used such that $\sigma_2/\sigma_1 \ll |ik_1 h_2|$. It is easy to see that a threshold frequency applies; however, given a conductivity contrast, a layer thickness can be always defined so that the solution holds to lower frequencies. In this regime, $\alpha_{1,2}$ in equation B-2 can be linearized, and thus, the equations for A and B simplify to

$$\alpha_{1,2} \sim \frac{1}{h_2}\left[-\frac{\sigma_2}{\sigma_1} \pm ih_2 k_1\left(1 + \frac{1}{2}\frac{\sigma_2^2}{(\sigma_1 ih_2 k_1)^2}\right)\right],$$

$$A \sim \frac{\sigma_1}{2ik_1}\left(1 + \frac{\sigma_2}{\sigma_1}ik_1 h_2\right),$$

$$B \sim -\frac{\sigma_1}{2ik_1}\left(1 - \frac{\sigma_2}{\sigma_1}ik_1 h_2\right). \quad \text{(B-3)}$$

Furthermore, using a small argument approximation for the Bessel functions ($J_0(\lambda_n r) \sim 1$ and $J_1(\lambda_n r) \sim \lambda_n r/2$ after Abramowitz and Stegun [1972]) and replacing equations. B-3 and B-2 into equation B-1, the vertical component of the electric field yields
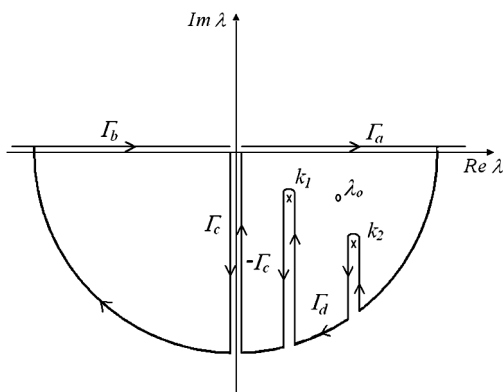

Figure B-1. Integration paths around the resistive layer pole λ_0, and branch points k_1 and k_2.

$$E_z^{(S)} = E_z^{(A)} + E_z^{(B)},$$

$$E_z^{(A)} = \frac{Ids}{4\pi\sigma_1}\left(\frac{\pi^4 \sigma_2^4}{8\sigma_1^4}\right)\sum_{n=0}^{\infty}\frac{p_n^3}{C_n - 1}\left[\frac{ik_1 + \sigma_1/(\sigma_2 h_2)}{ik_1 + \sigma_2/(\sigma_1 h_2(C_n - 1))}\right](ik_1)^3 e^{-ik_1(h-z)C_n},$$

$$E_z^{(B)} = \frac{Ids}{4\pi\sigma_1}\left(\frac{\pi^4 \sigma_2^4}{8\sigma_1^4}\right)\sum_{n=0}^{\infty}\frac{p_n^3}{C_n + 1}\left[\frac{ik_1 - \sigma_1/(\sigma_2 h_2)}{ik_1 + \sigma_2/(\sigma_1 h_2(C_n + 1))}\right](ik_1)^3 e^{-ik_1(h-z)C_n},$$

$$p_n = 2n + 1,$$

$$C_n = \left(1 + \frac{p_n^2 \pi^2 \sigma_2}{4\sigma_1}\right)^{1/2}. \quad \text{(B-4)}$$

As shown in Figure 4a, the equation B-4 results in excellent agreement with semianalytical estimates of the Bessel-Fourier convolution integral, and thereby, it is suitable to obtain analytical expressions for the time-domain response, assuming that the thick-layer, high-contrast approximation holds.

The response of the layer to a step on excitation is given by the inverse Laplace transform of $E_x^{(A,B)}/i\omega$, as $1/i\omega$ is the frequency domain expression of the Heaviside step function. After some algebra the inverse transforms

$$L^{-1}\left\{\frac{e^{-\gamma s^{1/2}}}{s^{1/2} + \alpha}\right\} = \frac{e^{-\gamma^2/4t}}{\sqrt{\pi t}} - \alpha e^{\alpha\gamma + \alpha^2 t}erfc\left(\alpha\sqrt{t} + \frac{\gamma}{2\sqrt{t}}\right),$$

$$L^{-1}\left\{\frac{s^{1/2}e^{-\gamma s^{1/2}}}{s^{1/2} + \alpha}\right\} = -\frac{\partial}{\partial\gamma}L^{-1}\left\{\frac{e^{-\gamma s^{1/2}}}{s^{1/2} + \alpha}\right\} \quad \text{(B-5)}$$

(Abramowitz and Stegun, 1972) will be needed, with the variable of integration defined as $s = i\omega$. The solution for $e_z^{(A)} = L^{-1}\{E_z^{(A)}/i\omega\}$ is then

$$e_z^{(A)} = \frac{Ids}{4\pi\sigma_1}\left(\frac{\pi^4 \sigma_2^4}{8\sigma_1^4}\right)\sum_{n=0}^{\infty}E_n\left\{\frac{F_n}{\sqrt{\pi t}}e^{-\gamma_n^2/4t}\right.$$

$$\left. - G_n e^{\alpha_n\gamma_n + \alpha_n^2 t}erfc\left(\alpha_n\sqrt{t} + \frac{\gamma_n}{2\sqrt{t}}\right)\right\}, \quad \text{(B-6)}$$
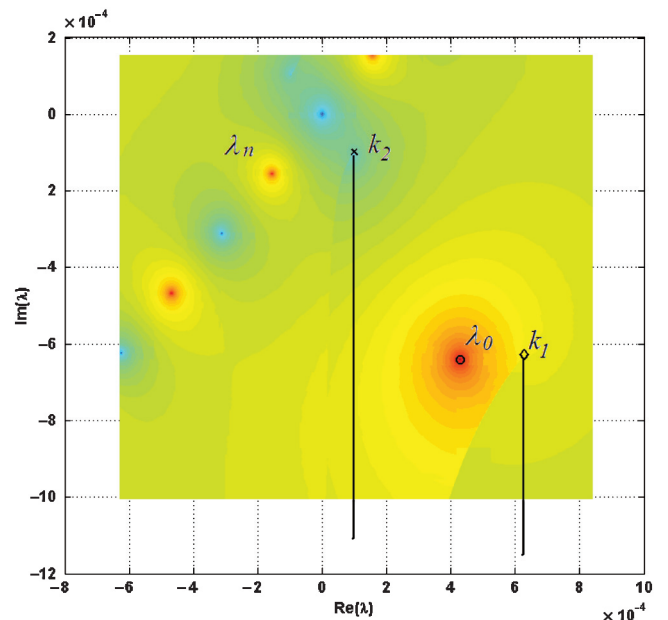

Figure B-2. Complex plane of λ of the modulated kernel.

where

$$
F_n = (\mu_0\sigma_1)^{3/2}\alpha_n^2\left[1 - \frac{1}{2\alpha_n^2 t} - \frac{\gamma_n}{4\alpha_n t} + \frac{\gamma_n^2}{4\alpha_n^2 t^2}\right.
$$
$$
\left. + \frac{b}{(\mu_0\sigma_1)^{1/2}}\left(\frac{\gamma_n}{2\alpha_n^2 t} - \frac{1}{\alpha_n}\right)\right],
$$
$$
G_n = (\mu_0\sigma_1)^{3/2}\alpha_n^3\left(1 - \frac{b}{(\mu_0\sigma_1)^{1/2}\alpha_n}\right),
$$
$$
E_n = \frac{p_n^3}{C_n - 1}, \tag{B-7}
$$

with

$$
\alpha_n = \frac{1}{(\mu_0\sigma_1)^{1/2}}\frac{\sigma_2}{\sigma_1 h_2(C_n - 1)},
$$
$$
\gamma_n = (\mu_0\sigma_1)^{1/2}C_n(h - z), \quad \text{and}
$$
$$
b = \frac{\sigma_1}{\sigma_2 h_2}. \tag{B-8}
$$

The solution for $e_z^{(B)} = L^{-1}\{E_z^{(B)}/i\omega\}$ is obtained from B-6 by re-defining

$$
\alpha_n = \frac{1}{(\mu_0\sigma_1)^{1/2}}\frac{\sigma_2}{\sigma_1 h_2(C_n + 1)},
$$
$$
b = -\frac{\sigma_1}{\sigma_2 h_2}, \quad \text{and}
$$
$$
E_n = \frac{p_n^3}{C_n + 1}. \tag{B-9}
$$

The total field is obtained by superimposing all of the contributions

$$
e_z(t) = L^{-1}\left\{\frac{E_z^{(D)}}{i\omega}\right\} - L^{-1}\left\{\frac{E_z^{(I)}}{i\omega}\right\} + L^{-1}\left\{\frac{E_z^{(A)}}{i\omega}\right\}
$$
$$
+ L^{-1}\left\{\frac{E_z^{(B)}}{i\omega}\right\}, \tag{B-10}
$$

where the direct and image terms $L^{-1}\{E_z^{(D,I)}/i\omega\}$ are (Ward and Hohmann (1988), equation. 2.50)

$$
e_z^{(D,I)}(t) = \frac{Ids}{4\pi\sigma_1 R^3}\left\{\left[\left(\frac{4}{\pi^{1/2}}\theta^3 R^3 + \frac{6}{\pi^{1/2}}\theta R\right)e^{-\theta^2 R^2} + 3erfc(\theta R)\right]\frac{(\Delta z)^2}{R^2}\right.
$$
$$
\left. - \left[\left(\frac{4}{\pi^{1/2}}\theta^3 R^3 + \frac{2}{\pi^{1/2}}\theta R\right)e^{-\theta^2 R^2} + erfc(\theta R)\right]\right\},
$$
$$
\theta = \left(\frac{\mu_0\sigma_1}{4t}\right)^{1/2} \tag{B-11}
$$

for a step on source time function, with $R = (x^2 + (\Delta z)^2)^{1/2}$, and $\Delta z = z + h$, $z - h$ for the source and image components, respectively.

SOLUTION FOR A HED EXCITATION

In light of the analysis presented in the previous discussion, a comparison with the mechanism giving rise to the horizontal component of the fields due to a HED excitation is in order.

Consider first the expression (in equation 3) for the secondary horizontal field of the *TM* mode

$$
E_x^{(\text{TM})} = \frac{Ids}{4\pi\sigma_1}\int_0^\infty 2\left[1 - \frac{Z_1}{Z_1 + \hat{Z}_2}\right]u_1 e^{-u_1(h-z)}
$$
$$
\left(\frac{J_1(\lambda r)}{r} - \lambda J_0(\lambda r)\right)d\lambda. \tag{B-12}
$$

Assuming that within the near offsets of interest the approximations $J_1(\lambda r) \sim \lambda r/2$ and $J_0(\lambda r) \sim 1$ hold, then equation B-12 can be rewritten as

$$
E_x^{(\text{TM})} = -\frac{Ids}{4\pi\sigma_1}\int_0^\infty u_1\lambda e^{-u_1(h-z)}d\lambda + \frac{Ids}{4\pi\sigma_1}\frac{1}{2}\int_0^\infty\left[\frac{2Z_1}{Z_1 + \hat{Z}_2}\frac{\lambda^3}{u_1}\right]
$$
$$
e^{-u_1(h-z)}\left(1 - \frac{k_1^2}{\lambda^2}\right)d\lambda. \tag{B-13}
$$

The first integral (namely, I_1) can be evaluated exactly. Noticing that $u_1 = (\lambda^2 - k_1^2)^{1/2}$, such that $u_1 du_1 = \lambda d\lambda$, and changing the integration variable to $\tau = u_1 - ik_1$, then the first term can be written as

$$
I_1^{(\text{TM})} = -\frac{Ids}{4\pi\sigma_1}\int_0^\infty u_1\lambda e^{-u_1(h-z)}d\lambda
$$
$$
= -\frac{Ids}{4\pi\sigma_1}e^{-ik_1(h-z)}\int_0^\infty(\tau + ik_1)^2 e^{-(h-z)\tau}d\tau. \tag{B-14}
$$

The integration represents a Laplace type of transform to the $s = (h - z)$ domain, thereby using Laplace transform tables (Abramowitz and Stegun, 1972)

$$
I_1^{(\text{TM})} = -\frac{Ids}{4\pi\sigma_1}e^{-ik_1(h-z)}\left[\frac{2}{(h-z)^3} + \frac{2ik_1}{(h-z)^2} - \frac{k_1^2}{(h-z)}\right], \tag{B-15}
$$

which resembles that of the main image term (equation 14). In fact, as frequency approaches DC, equation B-15 doubles the amplitude of the image term, but in the opposite direction.

The second term

$$
I_2^{(TM)} = \frac{Ids}{4\pi\sigma_1}\frac{1}{2}\int_0^\infty\left[\frac{2Z_1}{Z_1 + \hat{Z}_2}\frac{\lambda^3}{u_1}\right]e^{-u_1(h-z)}\left(1 - \frac{k_1^2}{\lambda^2}\right)d\lambda \tag{B-16}
$$

is analogous to the secondary fields, resulting from the VED excitation, i.e., the last term in the first of equation 1, but weighted by the factor $1 - k_1^2/\lambda^2$. Following the Kernel Modulation approach,

the resulting expression for I_2 is the same as that of equation B-4 (or equation B-6), but weighted by the factor $1 - k_1^2/\lambda_n^2$, i.e.,

$$I_2^{(\text{TM})} = \frac{Ids}{4\pi\sigma_1}(-2\pi i)\frac{k_2}{2}\sum_{n=0}^{\infty}\left(\frac{Z_1}{Z_1 + \hat{Z}_2}\right)_{\lambda=\lambda_n}$$
$$\frac{\lambda_n^3}{u_{1n}}\left(1 - \frac{k_1^2}{\lambda_n^2}\right)e^{-u_{1n}(h-z)}. \quad \text{(B-17)}$$

The weighting factor in each term on the summation can be written as

$$\left(1 - \frac{k_1^2}{\lambda^2}\right)_{\lambda=\lambda_n} = 1 + \frac{1}{p_n^2}\left(\frac{\sigma_1}{\sigma_2}\frac{4}{\pi^2}\right) \quad \text{(B-18)}$$

in each term of the summation. In the late times, increasing values of p_n in the summation dominate, the weighting factor B-18 tends to unity and the response approaches that of the VED excitation. In other words, the late time behavior of the TM fields resembles that of the fields due to $E_z^{(S)}$.

Consider now the TE mode of the fields. Assuming that at close source-receiver offsets $J_1(\lambda r) \sim 1/2\lambda r$ holds, the expression of the scattered fields (equation 4) simplifies to

$$E_x^{(\text{TE})} = -\frac{Ids}{4\pi\sigma_1}\frac{k_1^2}{i\omega\mu_0}\int_0^{\infty}\frac{\lambda}{Y_1 + \hat{Y}_2}e^{-u_1(h-z)}\mathrm{d}\lambda. \quad \text{(B-19)}$$

Using equation A-37, the kernel of the integrand is written as

$$\frac{1}{i\mu_0\omega}\frac{1}{Y_1 + \hat{Y}_2} \sim \frac{1}{2h_2(\alpha_2 - \alpha_1)}\left[-\frac{1 + \alpha_1 h_2}{u_1 - \alpha_1} + \frac{1 + \alpha_2 h_2}{u_1 - \alpha_2}\right]$$
$$\alpha_{1,2} = \frac{1}{2h_2}\left[-1 \pm (1 + 2\Delta^2 h_2^2)^{1/2}\right];$$
$$\Delta^2 = k_2^2 - k_1^2, \quad \text{(B-20)}$$

which yields

$$E_x^{(\text{TE})} = -\frac{Ids}{4\pi\sigma_1}\frac{k_1^2}{2h_2(\alpha_2 - \alpha_1)}\left[-(1 + \alpha_1 h_2)\int_0^{\infty}\frac{\lambda}{u_1 - \alpha_1}e^{-u_1(h-z)}\mathrm{d}\lambda\right.$$
$$\left. + (1 + \alpha_2 h_2)\int_0^{\infty}\frac{\lambda}{u_1 - \alpha_2}e^{-u_1(h-z)}\mathrm{d}\lambda\right] \quad \text{(B-21)}$$

The two integrals are solved separately, as before, using the change of variable $\tau = u_1 - ik_1$. To evaluate the first term, notice that $|\alpha_1| \ll |ik_1|$ if $|ik_1 h_2| \ll 2$, i.e., for wavelengths longer than h_2, those driving the late time behavior of the fields. In this case,

$$I_1^{(\text{TE})} = \int_0^{\infty}\frac{\lambda}{u_1 - \alpha_1}e^{-u_1(h-z)}\mathrm{d}\lambda \sim e^{-ik_1(h-z)}\int_0^{\infty}e^{-\tau(h-z)}\mathrm{d}\tau$$
$$= \frac{e^{-ik_1(h-z)}}{(h-z)}. \quad \text{(B-22)}$$

To evaluate the second term, the same change of variable is implemented. In this case, it is noticed that $|-\alpha_2 + ik_1| \gg \tau$, within the range of τ of dominant contribution to the integrand. In this case,

$$I_2^{(TE)} = \int_0^{\infty}\frac{\lambda}{u_1 - \alpha_2}e^{-u_1(h-z)}\mathrm{d}\lambda$$
$$\sim \frac{e^{-ik_1(h-z)}}{(-\alpha_2 + ik_1)^2}\int_0^{\infty}[\tau^2 + \tau(-\alpha_2 + 2ik_1)$$
$$+ ik_1(-\alpha_2 + ik_1)]e^{-\tau(h-z)}\mathrm{d}\tau$$
$$= \frac{e^{-ik_1(h-z)}}{(-\alpha_2 + ik_1)^2}\left[\frac{2}{(h-z)^3} + \frac{(-\alpha_2 + 2ik_1)}{(h-z)^2}\right.$$
$$\left. + \frac{ik_1(-\alpha_2 + ik_1)}{(h-z)}\right]. \quad \text{(B-23)}$$

The final expression for the fields is then obtained by replacing equations B-22 and B-23 in equation B-21. Further simplification is attained by noticing to a good approximation that $\alpha_2 \sim -1/h_2$, $1 + \alpha_2 \sim \Delta^2 h_2^2$ and $\alpha_1 \sim 0$, and that $\Delta^2 \sim -k_1^2$ when a strong conductivity contrast applies. In this case,

$$E_x^{(\text{TE})} = -\frac{Ids}{4\pi\sigma_1}\frac{k_1^2}{2\alpha_2 h_2}e^{-ik_1(h-z)} + \frac{Ids}{4\pi\sigma_1}\frac{k_1^4 h_2^4}{2}e^{-ik_1(h-z)}$$
$$\left(\frac{2}{(h-z)^3} + \frac{1}{h_2(h-z)^2} + \frac{ik_1}{h_2(h-z)}\right), \quad \text{(B-24)}$$

where the first and second terms are obtained from $I_1^{(\text{TE})}$ and $I_2^{(\text{TE})}$, respectively. Inspection indicates that the first term dominates, and furthermore, the product $|\alpha_2 h_2| \sim 1$ and thereby the TE mode has but negligible dependence on the layer parameters. Furthermore, the linear dependence in k_1^2 indicates that as the frequency vanishes (or at very late times) so does the TE component of the field, which represents the inductive character of this mode.

To test the accuracy of the expressions described above, the solutions represented by equation B-24 for the TE mode, and the superposition of equations B-15 and B-17 for the TM mode is compared with the semianalytical evaluation of the integrals in Figure 6. The agreement is evident (see symbols compared to lines).

Time-domain expressions are obtained as before, assuming a step on source time function, i.e., a $(i\omega)^{-1}$ weight is multiplied to each of the equations in 25, and suitable inverse Laplace transforms are performed:

$$e_x(t) = L^{-1}\left\{\frac{E_x^{(D)}}{i\omega}\right\} - L^{-1}\left\{\frac{E_x^{(I)}}{i\omega}\right\} + L^{-1}\left\{\frac{E_x^{(TE)}}{i\omega}\right\}$$
$$+ L^{-1}\left\{\frac{E_x^{(TM)}}{i\omega}\right\}. \quad \text{(B-25)}$$

The direct and main image components are available in Ward and Hohmann (1988) (equation 2.50) which yields

$$e_x^{(D)} = \frac{Ids}{4\pi\sigma_1}\frac{2}{r^3}\left(\frac{2\theta r}{\pi^{1/2}}e^{-\theta^2 r^2} - erfc(\theta r)\right),$$

$$\theta = \left(\frac{\mu_0\sigma_1}{4t}\right)^{1/2} \qquad\qquad \text{B-26}$$

for the direct term and

$$e_x^{(I)} = \frac{Ids}{4\pi\sigma_1}\frac{1}{(h-z)^3}\left[\left(\frac{4\theta^3(h-z)^3}{\pi^{1/2}} + \frac{2\theta(h-z)}{\pi^{1/2}}\right)e^{-\theta^2(h-z)^2}\right.$$

$$\left. + erfc(\theta(h-z))\right] \qquad\qquad \text{(B-27)}$$

for image term, assuming that the radial distance $r \ll (h-z)$. The inverse Laplace's transform of the TE field ($E_x^{(TE)}$) yields,

$$e_x^{(TE)} = -\frac{Ids}{4\pi\sigma_1}\frac{1}{(h-z)^3}\left(\frac{2\theta^3(h-z)^3}{\pi^{1/2}}\right)e^{-\theta^2(h-z)^2}, \quad \text{(B-28)}$$

whereas the transform of the TM field ($E_x^{(TM)}$) provides

$$e_x^{(TM)} = \frac{Ids}{4\pi\sigma_1}\frac{1}{(h-z)^3}\left[\left(\frac{4\theta^3(h-z)^3}{\pi^{1/2}} + \frac{4\theta(h-z)}{\pi^{1/2}}\right)\right.$$

$$\left. e^{-\theta^2(h-z)^2} + 2erfc(\theta(h-z))\right] + e_x^{(TMS)}(t), \qquad \text{(B-29)}$$

where the secondary layer response term $e_x^{(TMS)}(t)$ is the Laplace's transform of $E_x^{(TMS)}$ in equation 25. A suitable expression for $e_x^{(TMS)}(t)$ can be readily obtained by computing the transform of each harmonic in equation B-17. As noted before, equation B-17 is a weighted version of the solution for E_z due to a VED in equation B-1. Therefore, the time-domain expression of the field due to the HED is the same as that describing $e_z^{(A,B)}(t)$ in equation B-6, weighted accordingly by the factor (equation B-18).

To check the validity of the solution, an expression for the scattered field is obtained by superimposing the components in equations B-27, B-28, and B-29, which is subtracted from its asymptotic late time limit to render the step off transient behavior:

$$e_x^{(SC)} = (e_x^I + e_x^{TM} + e_x^{TE})_{t\to\infty} - (e_x^I + e_x^{TM} + e_x^{TE}),$$

$$e_x^{(SC)} = -\frac{Ids}{4\pi\sigma_1}\frac{1}{(h-z)^3}\left[1 - \left(\frac{2\theta^3(h-z)^3}{\pi^{1/2}} + \frac{2\theta(h-z)}{\pi^{1/2}}\right)\right.$$

$$\left. e^{-\theta^2(h-z)^2} - erfc(\theta(h-z))\right] - e_x^{(TMS)}(t). \qquad \text{(B-30)}$$

Figure 7a shows the agreement between semianalytical estimates of the scattered fields (symbols) and the analytical eqation B-30, and the individual components of the solution for the scattered field are shown in Figure 7b.

SUPERPOSITION OF IMAGES

At this point, the kernel modulation expressions (equation B-4 for the VED and equation B-17 for the HED) provide a solution for the fields describing a superposition of an infinite series of harmonics, which agree to a great degree with the semianalytical

evaluation of the integrals. However, further analysis is required to interpret them in light of the structure of the fields in the near-offset regime. In other words, it is not evident that equations B-4 or B-17 represent the concept of a superposition of images described by the asymptotic solutions. In what follows, equation B-4 (the same analysis applies for equation B-17) is interpreted by analyzing its behavior at the 0th order, as well as in the limit as $n \to \infty$.

Consider first $n = 0$, such that $p_n = 1$ and $C_n \to 1$. Notice that $C_n \sim 1$ as long as $\sigma_2/\sigma_1 \ll (\pi p_n/2)^2$, and thereby, the simplifications that follow can be done for higher harmonics as well. After some simple algebra, the 0th harmonic of the total field ($E_z^{(S)} = E_z^{(A)} + E_z^{(B)}$) can be written as

$$E_z^{(S)} = \frac{Ids}{4\pi\sigma_1}\left(\frac{\pi^4\sigma_2^4}{8\sigma_1^4}\right)(ik_1)^3\left[\frac{1}{2} - \frac{\sigma_1}{\sigma_2}\left(\frac{1}{2ik_1h_2} - ik_1h_2\right)\right.$$

$$\left. + \left(\frac{\sigma_1}{\sigma_2}\right)^2\right]e^{-ik_1(h-z)}. \qquad \text{(B-31)}$$

In the previous section, it was shown that the asymptotic expressions were accurate in as much as $|ik_1(h-z)| \gg 1$. Thus, let us assume that $ik_1(h-z) \sim O(1)$, i.e., the 0th order, is most important for those wavelengths on the order of the distance to the layer. For higher frequencies, the exponential decay dominates, whereas for lower frequencies (even longer wavelengths), the $(ik_1)^3$ dominates; in either case, the field decreases. Under this assumption, it is justified to replace $ik_1 \sim (h-z)^{-1}$, and thereby equation B-31 simplifies to

$$E_z^{(S)} \sim \frac{Ids}{4\pi\sigma_1}\frac{\pi^4}{16}\left(\frac{\sigma_2}{\sigma_1}\right)^2\frac{e^{-ik_1(h-z)}}{(h-z)^3}2\left[1 + ik_1h_2\frac{\sigma_2}{\sigma_1}\right]. \quad \text{(B-32)}$$

This expression represents the dipolar character of an image source at near offsets, similar to that described by $E_z^{(S)}$ in equation 9.

Consider now the upper limit, i.e., $n \to \infty$. In this scenario, let us assume that for some value of $n > n_0$,

$$p_n > p_0 = 2n_0 + 1, \qquad C_n \to \frac{p_n\pi}{4}\left(\frac{\sigma_2}{\sigma_1}\right)^{1/2}. \qquad \text{(B-33)}$$

In this case, the secondary field can be written as

$$E_z^{(S)} \sim \frac{Ids}{4\pi\sigma_1}\left(\frac{\pi\sigma_2}{2\sigma_1}\right)^4\frac{\pi}{4}\left(\frac{\sigma_2}{\sigma_1}\right)^{1/2}(ik_1)^3\sum_{n=n_0}^{\infty}p_n^2 e^{-i\alpha p_n}\Delta p_n, \qquad \text{(B-34)}$$

where

$$\alpha = k_1(h-z)\frac{\pi}{4}\left(\frac{\sigma_2}{\sigma_1}\right)^{1/2}. \qquad \text{(B-35)}$$

In equation B-34, the Δp_n factor in the summation has been arbitrarily introduced for convenience, as in fact $\Delta p_n = 2$ exactly, and it represents the difference between two consecutive values of p_n. However, noticing that the summation is the discrete representation of and integration in p_n, it is justified to define the limiting behavior of the summation by

$$\sum_{n=n_0}^{\infty} p_n^2 e^{-i\alpha p_n} \Delta p_n \rightarrow \int_{p_0}^{\infty} p^2 e^{-i\alpha p} dp, \qquad (B\text{-}36)$$

where p replaces p_n to shorten the nomenclature.

Evaluating the integral yields the limiting expression

$$\lim_{n \to \infty} E_z^{(S)} \sim -\frac{Ids}{4\pi\sigma_1}\pi^2\left(\frac{\sigma_2}{\sigma_1}\right)^3 \frac{e^{-i\frac{p_0\pi}{4}k_2(h-z)}}{(h-z)^3} 2\left[1 + \frac{p_0\pi}{4}ik_2(h-z)\right.$$
$$\left. + \frac{(p_0\pi)^2}{32}(ik_2(h-z))^2\right], \qquad (B\text{-}37)$$

which also represents the dipolar character of an image source at near offsets, such as that described by $E_z^{(I)}$ in equation 9. Most importantly, the $ik_2(h-z)$ dependence observed in equation B-37 is indicative of an image source in a whole-space medium with the properties of the layer (σ_2), which is related to the charges induced in the lower boundary by the fields due to the charges in the upper boundary.

REFERENCES

Abramowitz, M., and I. Stegun, 1972, Handbook of mathematical functions with formulas, graphs and mathematical tables: National Bureau of Standards.

Anderson, W., 1979, Numerical integration of related Hankel transforms of order 0 and 1 by adaptive digital filtering: Geophysics, **44**, 1287–1305, doi: 10.1190/1.1441007.

Bannister, P. R., 1984, New simplified formulas for elf subsurface-to-subsurface propagation: IEEE Journal of Oceanic Engineering, **9**, 154–163, doi: 10.1109/JOE.1984.1145620.

Baños, A., 1966, Dipole radiation in the presence of a conducting half-space: Pergamon Press Inc.

Barsukov, P., F. E, and S. B, 2007, Method for hydrocarbon mapping and apparatus for use when performing the method: WIPO Patent WO 2007/053025 A1.

Chave, A. D., 2009, On the electromagnetic fields produced by marine frequency domain controlled sources: Geophysical Journal International, **179**, 1429–1457, doi: 10.1111/gji.2009.179.issue-3.

Cuevas, N., D. Alumbaugh, and H. F. Morrison, 2009, Analytical expressions for the electromagnetic fields for a 1D resistive layer in a conductive wholespace system: Presented at the 71st Annual International Conference and Exhibition, EAGE.

Eidesmo, T., S. Ellingsrud, L. M. MacGregor, S. Constable, M. C. Sinha, S. Johansen, F. N. Kong, and H. Westerdahl, 2002, Seabed logging (SBL), a new method for remote and direct identification of hydrocarbon filled layers in deepwater areas using controlled source electromagnetic sounding: First Break, **20**, 144–152.

Kaufman, A., 2010, Principles of electric methods in surface and borehole geophysics: Elsevier.

Kong, F., S. Johnstad, and J. Park, 2010, Wavenumber of the guided wave supported by a thin resistive layer in marine controlled-source electromagnetics: Geophysical Prospecting, **58**, 711–723, doi: 10.1111/gpr.2010.58.issue-4.

Loseth, L. O., 2007, Modelling of controlled source electromagnetic data: Ph.D. thesis, Norwegian University of Science and Technology.

Mittet, R., and T. Schaug-Pettersen, 2008, Shaping optimal transmitter waveforms for marine CSEM surveys: Geophysics, **73**, no. 3, F97–F104, doi: 10.1190/1.2898410.

Morse, P., and H. Feshbach, 1953, Methods of theoretical physics: McGraw-Hill Book Co.

Sharma, P., 1997, Environmental and engeneering geophysics: Cambridge University Press.

Swidinsky, A., and R. N. Edwards, 2009, The transient electromagnetic response of a resistive sheet: Straightforward but not trivial: Geophysical Journal International, **179**, 1488–1498, doi: 10.1111/gji.2009.179.issue-3.

Wait, J., 1960, Propagation of electromagnetic pulses in a homogeneous conducting earth: Applied Scientific Research, Section B, **8**, 213–253.

Ward, S. H., and G. W. Hohmann, 1988, Electromagnetic theory for geophysical applications , in M. N. Nabighian, ed., Electromagnetic methods in applied geophysics of Investigations in Geophysics no. 3: SEG, **1**, 131–311.

Weidelt, P., 2007, Guided waves in marine csem: Geophysical Journal International, **171**, 153–176, doi: 10.1111/gji.2007.171.issue-1.